LBL-12550 c.2
Preprint

Lawrence Berkeley Laboratory
UNIVERSITY OF CALIFORNIA

Materials & Molecular Research Division

MAY 21 1981
LIBRARY
DOCUMENTS

Submitted to Nuclear Technology

A MECHANISTIC ANALYSIS OF RUTHENIUM TRANSPORT IN UO_2

D.R. Olander

April 1981

TWO-WEEK LOAN COPY

This is a Library Circulating Copy which may be borrowed for two weeks. For a personal retention copy, call Tech. Info. Division, Ext. 6782

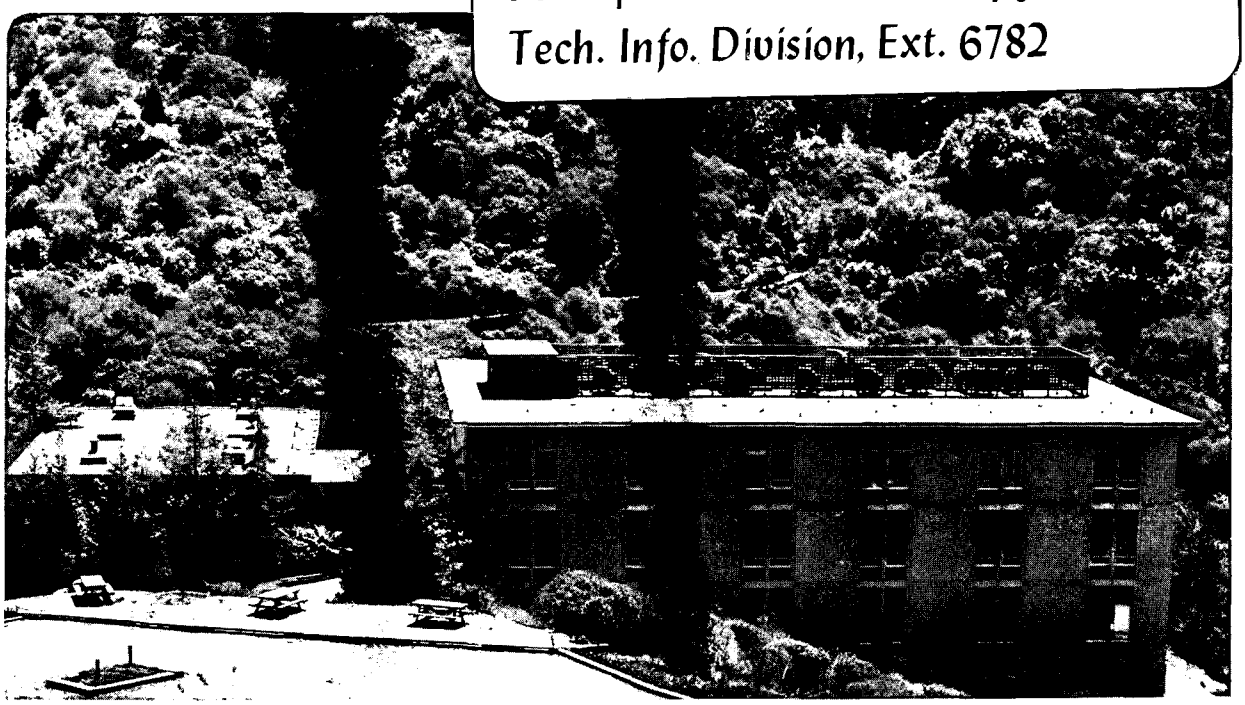

LBL-12550 c.2

Prepared for the U.S. Department of Energy under Contract W-7405-ENG-48

DISCLAIMER

This document was prepared as an account of work sponsored by the United States Government. While this document is believed to contain correct information, neither the United States Government nor any agency thereof, nor the Regents of the University of California, nor any of their employees, makes any warranty, express or implied, or assumes any legal responsibility for the accuracy, completeness, or usefulness of any information, apparatus, product, or process disclosed, or represents that its use would not infringe privately owned rights. Reference herein to any specific commercial product, process, or service by its trade name, trademark, manufacturer, or otherwise, does not necessarily constitute or imply its endorsement, recommendation, or favoring by the United States Government or any agency thereof, or the Regents of the University of California. The views and opinions of authors expressed herein do not necessarily state or reflect those of the United States Government or any agency thereof or the Regents of the University of California.

LBL-12550

A MECHANISTIC ANALYSIS OF RUTHENIUM TRANSPORT IN UO_2

D.R. Olander

Materials and Molecular Research
Division of the Lawrence Berkeley
Laboratory and the
Department of Nuclear Engineering
University of California Berkeley
Berkeley, California 94720

This work was supported by the Director, Office of Energy Research, Office of Basic Energy Sciences, Materials Sciences Division of the U.S. Department of Energy under contract # W-7405-ENG-48.

ABSTRACT

A detailed model of the interaction of ruthenium and urania is developed and compared to experimental data. The mechanism involves physical solution of the metal in the grain boundaries of the ceramic followed by simultaneous diffusion and chemical reaction to produce URu_3 intergranular inclusions. The process occurs only when the oxide is substoichiometric, reduction being effected by oxygen absorption by the refractory metal crucible containing the specimen. Reaction ceases when the URu_3 product in the grain boundary reaches a thickness which prevents removal of the other reaction product, oxygen. Fitting the model predictions to the experimental ruthenium spreading data from a source plane of the metal held between oxide pellets provides quantitative estimates of the parameters of the model. The theory also correctly predicts the shape and magnitude of ruthenium migration in UO_2 in a temperature gradient, in which thermal diffusion does not appear to play a significant role.

1. Introduction

The mobility and chemical state of the fission products in oxide fuels has a significant effect on performance. The behavior of the noble metal fission products, of which ruthenium is the principal contributor, is particularly puzzling; they precipitate in alloy form as micron-size particles in the hot regions of LMFBR fuel, yet they appear to have appreciable mobility because large ingots are recovered from the central void of irradiated fuels. In order to clarify this phenomenon, refractory and noble metal particles were tested in UO_2 in isothermal and temperature gradient anneals(1). The refractory metal particles (tungsten and molybdenum) did not chemically react with UO_2, nor did they move bodily in a temperature gradient. Ruthenium, on the other hand, dissolved and diffused into and reacted with hypostoichiometric urania in high temperature isothermal anneals. This element also showed extensive movement up a temperature gradient. The isothermal spreading data were adequately fitted by simple diffusion theory, but extension of this model to the thermal gradient migration data failed. A mechanism of the ruthenium-UO_2 interaction was suggested in Ref. 1. The purpose of the present study is to develop this model quantitatively, with the object of explaining not only the isothermal annealing results but the thermal gradient migration data as well.

In the experiments described in Ref. 1, specimens consisting of a layer of powdered ruthenium metal or a disk of massive ruthenium placed between a polished UO_2 pellet and a thin UO_2 wafer were annealed isothermally. After the anneal, the specimens were successively polished parallel to the interface, the exposed surface examined by microscope and the Ru/U ratio measured by X-ray fluorescence. By removing several tens of microns at a

time, the ruthenium concentration distribution was established. This distribution accurately fitted that expected for simple diffusion from an inexhaustible plane source in an infinite medium:

$$C(z,t) = \left(C_o\right)_{app} \operatorname{erfc}\left(\frac{z}{2\sqrt{D_{eff}t}}\right) \qquad (1)$$

where C is the atomic ratio of ruthenium to uranium, $\left(C_o\right)_{app}$ is an apparent ruthenium solubility in UO_2, D_{eff} is the effective diffusion coefficient of ruthenium in UO_2, and z is the distance (in either direction) from the source plane. Experiments were conducted in both molybdenum crucibles and tungsten crucibles at temperatures between 2330 and 2570 K. The apparent solubilities were the same for the two metals, but the effective diffusion coefficients were larger in molybdenum crucibles than in tungsten crucibles.

Microscopic examination of the surface exposed by polishing showed that the grain boundaries of the specimen contained a metallic phase (Fig. 6 of Ref. 1). Near the original interface between the pellets and wafer, the grain boundaries were completely filled (i.e., each grain was outlined by the metallic layer) but far from the interface, the metallic inclusions were separated in grain boundaries. Electron microprobe analysis showed that the inclusions contained both uranium and ruthenium, and it is assumed that the composition corresponds to the intermetallic compound URu_3. No ruthenium was detected within the grains of UO_2.

In addition to the isothermal anneals described above, several experiments in a temperature gradient of $\sim$ 1400 K/cm were conducted(1). Simple diffusion theory, even when the temperature-dependence of the diffusion coefficient and thermal diffusion were taken into account, failed to fit the measured ruthenium distributions. It therefore appears that the good agreement of the measured ruthenium spreading in isothermal

anneals with Eq(1) is fortuitous, and that the effective diffusion coefficient and apparent solubility have no physical meaning. This situation is analogous to that encountered in fission gas mobility in UO_2 where the trapping-diffusion model(2,3) provides a much better description of the phenomenon than does simple diffusion. Similarly, analysis of diffusion in polycrystalline bodies must consider grain boundary as well as volume diffusion(4). Diffusion of carbon in steel is often treated as a simple diffusion process(5), but detailed understanding of carburization can be achieved only by an analysis which involves carbide precipitation along with diffusion(6).

2. Isothermal Ruthenium Transport Model

The model described quantitatively in subsequent sections assumes that elemental ruthenium dissolves and diffuses atomically in the grain boundaries of UO_2. The source of ruthenium is the layer of powders or the disk placed in the interface between the two uranium dioxide pieces. This source is assumed to be inexhaustible and to generate an equilibrium concentration in the adjacent UO_2 denoted by ϕ_s g-atoms Ru/per cm^2 of grain boundary. If the UO_2 remained at its initial stoichiometric composition, the specimen would eventually become saturated with ruthenium on all grain boundaries, and the ruthenium-to-uranium ratio would be:

$$C_{sat} = \frac{A_{gb}\phi_s}{\rho_{UO_2}} \qquad (2)$$

where ρ_{UO_2} is the molar density of UO_2 and A_{gb} is the area of grain boundary per unit volume of polycrystalline oxide. The grains in UO_2 are modeled as tetrakaidecahedra, which is a space-filling polyhedron with 36 edges of length ℓ. Its 14 sides consist of 8 regular hexagons and 6 squares, so that the surface area is 26.78 ℓ^2. The volume is $8\sqrt{2}\ell^3$, and the diameter of a sphere

of the same volume (used to describe the grain size) is $d = 2.79\ \ell$. For this grain model, $A_{gb} = 3.30/d$.

The concentration given by Eq(2) is expected to be too small to detect. Rather, measurable quantities of ruthenium are introduced into the UO_2 at locations away from the original interface only by virtue of ruthenium diffusion in the grain boundaries and simultaneous reaction with the UO_2 to produce the URu_3 intermetallic compound. This can occur only with reduced UO_2. In the model, UO_2 reduction is assumed to occur by absorption of oxygen from the oxide by the refractory metal which contains the specimen. When the O/U ratio of the oxide reaches a critical value $(O/U)^*$, reaction to form URu_3 begins. The time at which this occurs is denoted by t^*. The refractory metal crucible continues to reduce the oxide and the URu_3 layers continue to grow in the grain boundaries of UO_2. However this process is limited by the oxygen permeability of the URu_3 layers which surround the grains.

Contrary to the crucible metals, which are body-centered cubic Mo or W, ruthenium or URu_3 has an fcc structure. Hence the permeability (i.e., diffusivity times solubility) of the latter for interstitial solutes such as oxygen is probably much smaller than that of Mo or W. Consequently, encapsulation of UO_2 grains by a complete layer of URu_3 isolates the grain from the reduction process occurring in the rest of the urania which is in direct communication with the refractory metal crucible. As a grain becomes isolated by its URu_3 shell, the oxygen liberated by the reaction to form URu_3 cannot be removed by transport to the refractory metal sinks. Thereafter the O/U ratio of isolated grains increases until the critical value $(O/U)^*$ is reached, when the reaction stops.

The oxygen conductance of the URu_3 layer is equal to the permeability of oxygen in the intermetallic compound divided by the layer thickness. As reaction proceeds and the layer grows, the conductance decreases as $(2\delta)^{-1}$, where δ is the

half-thickness of the layer. To simplify the analysis, it is assumed that all reaction stops when the half-thickness reaches a value δ_1, at which point the maximum ruthenium-to-uranium ratio is achieved. The latter is:

$$C_o = 2\delta_1 A_{gb}\left(\rho_{URu_3}/\rho_{UO_2}\right) \simeq \frac{6.6\ \delta_1}{d}\left(\rho_{URu_3}/\rho_{UO_2}\right) \qquad (3)$$

where ρ_{URu_3} is the number of gram atoms of ruthenium per unit volume of URu_3. Taking $d \simeq 150$ μm (characteristic of the experiments in which considerable grain growth occurred) and the density ratio of 2.5, a terminal half-layer thickness of 0.1 μm corresponds to an apparent solubility of ruthenium in UO_2 of ~ 1 a/o, which is typical of the values deduced in the experiments.

The apparent solubility is not a thermodynamic parameter at all; rather it is a reflection of the impermeability of URu_3 to oxygen, which prevents continued oxygen removal, and hence URu_3 formation, by the refractory metal sinks. However, C_o given by Eq(3) has properties which are consistent with the data reported in Ref. 1. First, the value of C_o is independent of the crucible metal, which may affect the time at which the blocking layer thickness is attained but not the value of δ_1 proper. Thus, the observation that C_o is the same in Mo and W crucibles is understandable. Second, the activation energy of C_o is that of the blocking layer thickness, δ_1. If one recognizes that the oxygen transport conductance of the URu_3 layer varies as the ratio of the permeability to the thickness, the value of δ needed to effectively stop oxygen transfer increases as the permeability increases. Hence δ_1 should exhibit the same temperature dependence as the product of the diffusivity and solubility of oxygen in URu_3.

The time at which the blocking layer thickness δ_1 is reached at the source plane (z = 0) is denoted by t_1. Thereafter, layers surrounding

grains away from the interface attain thickness δ_1, so that a band of UO_2 "saturated" with ruthenium expands from the original interface. The outer edge of this "saturated" zone is denoted by z_1 and is a function of time starting from $z_1 = 0$ at $t = t_1$. Reaction continues in the region $z > z_1$, but the zone $0 \leq z \leq z_1$ simply acts as a pure resistance to grain boundary transport of ruthenium moving from the source plane at $z = 0$ to the reaction region at $z > z_1$.

The above model is treated quantitatively below. In section 3, the thermodynamics and kinetics of the grain boundary reaction which produces URu_3 are modeled. The rate of reduction of the UO_2 by the refractory metal crucible used as a container is modeled in Section 4. Transport of ruthenium in the grain boundaries of the UO_2, both with and without reaction to form URu_3, is treated in Section 5. Calculation of the thickness of the URu_3 layer as a function of time and position is performed in Section 6 and data analysis is presented in Section 7. Experiments in a temperature gradient are considered in Section 8.

3. Thermochemistry and Reaction Kinetics of URu_3 Production

URu_3 forms only when the oxide is hypostoichiometric. Thermochemically, Ru, URu_3, and UO_{2-x} can coexist only when the reaction:

$$3Ru + UO_{2-x} = URu_3 + \left(\frac{2-x}{2}\right) O_2 \qquad (4)$$

is at equilibrium. The critical oxygen pressure required for the equilibrium is given by:

$$\left(P^*_{O_2}\right)^{\frac{2-x}{2}} = \exp\left[\frac{\Delta G^\circ_{fUO_{2-x}} - \Delta G^\circ_{fURu_3}}{RT}\right] \qquad (5)$$

where $\Delta G^\circ_{fUO_{2-x}}$ is the standard free energy of formation of UO_{2-x} and

$\Delta G^{\circ}_{fURu_3}$ is that of URu_3. The critical oxygen pressure corresponds to a critical O/U ratio via the oxygen potential of UO_{2-x}:

$$\overline{\Delta G_{O_2}} = RT\ln p_{O_2}$$

which is known. Thus, $p^*_{O_2}$ $\left(\text{or}(O/U)^*\right)$ is a function of temperature only (1).

In the model, the rate of reaction (4) is one of the slow steps in the overall process. The actual reaction occurs between uranium in UO_{2-x} and ruthenium present in the interface between the urania and the growing layer of intermetallic compound, in which ruthenium is assumed to be insoluble. Thus, we consider the slow, reversible chemical reaction:

$$U(\text{in } UO_{2-x}) + 3Ru(\text{in interface}) \underset{k_F}{\overset{k_R}{\rightleftharpoons}} URu_3(\text{pure layer}) \qquad (6)$$

where the foward and reverse rate constants are related by the equilibrium requirement:

$$\frac{k_F}{k_R} = \exp\left[-\frac{\Delta G^{\circ}_{fURu_3}}{RT}\right] \qquad (7)$$

We assume that the foward and reverse rate expressions are consistent with small departures from equilibrium, or:

$$R_F = k_F a_U a_{Ru}^3$$

$$R_R = k_R a_{URu_3} \qquad (8)$$

where a_i is the activity of species i.

Because the intermetallic phase is assumed to be pure, $a_{URu_3} = 1$, and the net rate of reaction per unit of grain boundary area is

$$J_{URu_3} = k_F a_U a_{Ru}^3 - k_R = k_R \left[a_U a_{Ru}^3 (k_F/k_R) - 1 \right] \tag{9}$$

The activity of uranium in UO_{2-x} can be obtained by consideration of the reaction:

$$U + \left(\frac{2-x}{2}\right) O_2 = UO_{2-x} \tag{10}$$

Application of the Gibbs-Duhem relation yields:

$$d\ln a_U + \left(\frac{2-x}{2}\right) d\ln p_{O_2} = 0 \tag{11}$$

or, in integrated form:

$$a_U = p_{O_2}^{-\left(\frac{2-x}{2}\right)} \exp\left[\frac{\Delta G^\circ_{fUO_{2-x}}}{RT}\right] \tag{12}$$

Substitution of Eqs(12), (7), and (5) into Eq(9) yields:

$$J_{URu_3} = k_R \left[\left(\frac{p^*_{O_2}}{p_{O_2}} \right)^{\frac{2-x}{2}} a_{Ru}^3 - 1 \right] \tag{13}$$

Photomicrographs of the region of UO_2 into which ruthenium had penetrated revealed patchy coverage of URu_3 in the grain boundary with the remainder of the interface bare(Fig. 6 of Ref. 1). Only near the source plane were the UO_2 grain boundaries completely filled with the intermetallic compound. Thus we set $a_{Ru} = 1$ in Eq. (13), but because of the discontinuous coverage at the interface, assume that the reaction proceeds only over a fraction ε of the interface. The rate per unit of total interface area is then:

$$J_{URu_3} = \varepsilon\, k_R \left[\left(p^*_{O_2}/p_{O_2} \right)^{\frac{2-x}{2}} - 1 \right] \tag{14}$$

The fractional coverage of the interface by ruthenium patches is related to the average Ru concentration at the interface by the empirical function:

$$\varepsilon = 1 - e^{-b\phi} \tag{15}$$

where b is a constant. Substituting Eq. (15) into Eq. (14) yields:

$$J_{URu_3} = k_R \left(1 - e^{-b\phi}\right) \left[\left(p^*_{O_2}/p_{O_2} \right)^{\frac{2-x}{2}} - 1 \right] \tag{16}$$

The rate of the interfacial chemical reaction described by Eq. (16) is consistent with equilibrium limitations; J_{URu_3} is zero if the oxide is insufficiently hypostoichiometric $\left[p_{O_2} \geq \left(p_{O_2} \right)^* \right]$ of if no elemental ruthenium is present in the grain boundary ($\phi = 0$).

4. <u>The O/U Ratio of the Uranium Phase</u>

The oxygen content of the urania phase changes during the anneal because of:

i) oxidation due to URu_3 formation,

and ii) reduction due to absorption of oxygen by the refractory metal crucible.

The first of these can be shown to be negligible, so the O/U ratio of the sample is assumed to be controlled by absorption of oxygen by the refractory metal fittings which contact the specimen. The metal is represented by a semi-infinite medium into which oxygen diffuses from an interface where

the UO_{2-x} maintains an oxygen concentration in the metal given by Sievert's law:

$$c(0,t) = c_o(t) = S_M\sqrt{p_{O_2}} \tag{17}$$

where $c(y,t)$ is the oxygen concentration at depth y into the metal at time t, S_M is the solubility coefficient of oxygen in the metal and p_{O_2} is the partial pressure of oxygen corresponding to the current O/U ratio and temperature of the urania phase in contact with the metal.

The oxygen diffusion equation in the metal is:

$$\frac{\partial c}{\partial t} = D_M \frac{\partial^2 c}{\partial y^2} \tag{18}$$

where D_M is the diffusivity of oxygen in the metal. The initial condition is:

$$c(y,0) = 0$$

and the boundary conditions are:

$$c(0,t) = c_o(t)$$

$$c(\infty,t) = 0$$

A good approximate solution of this equation for the gradient at y = 0 is(7):

$$\left(\frac{\partial c}{\partial y}\right)_{y=0} = -\frac{c_o(t)}{\sqrt{\pi D_M t}} - \sqrt{\frac{t}{\pi D_M}}\,\frac{dc_o}{dt}$$

and the rate of absorption of oxygen by the metal surrounding the specimen is:

$$R_M = -A_c D_M (\partial c/\partial y)_0$$

where A_c is the total area of contact between the sample and the metal.

An oxygen balance on the urania gives:

$$\frac{d(O/U)}{dt} = - \frac{R_M}{V_p \, \rho_{UO_2}}$$

where V_p is the volume of the UO_2 pellet.

Combining the preceeding equations yields:

$$\frac{d(O/U)}{dt} = - \frac{A_c S_M \sqrt{D_M}}{\sqrt{\pi} \, V_p \, \rho_{UO_2}} \left[\frac{\sqrt{p_{O_2}}}{\sqrt{t}} + \sqrt{t} \, \frac{d\sqrt{p_{O_2}}}{dt} \right]$$

Defining dimensionless variables:

$$\zeta = \frac{A_c S_M \sqrt{D_M} \, \sqrt{p^*_{O_2}}}{\sqrt{\pi} \, V_p \rho_{UO_2}} \sqrt{t} \qquad (19)$$

and

$$Y = (p_{O_2}/p^*_{O_2})^{\frac{1}{2}}$$

yields:

$$\frac{d(O/U)}{d\zeta} = - \frac{2Y}{1 + \zeta \, dY/d(O/U)} \qquad (20)$$

For a specified temperature $p^*_{O_2}$ is known from the thermochemical analysis of Section 3 and p_{O_2} is a known function of O/U by the thermochemistry of urania. Hence, the variable Y is a specified function of O/U and Eq(20) can be integrated numerically with an initial condition giving the oxygen-to-metal ratio of the specimen at the start of the anneal (assumed to be 2.00). The form of the solution convenient for use in the rate expression of Eq(16) is:

$$f(\zeta) = \left(p^*_{O_2}/p_{O_2} \right)^{\frac{2-x}{2}} - 1 \qquad (21)$$

Assuming the initial urania specimen to be perfectly stoichiometric, a time t^* is required before $f(t) \gtrsim 0$ and the reaction to form URu_3 becomes thermodynamically possible. Numerical solutions of Eq.(20) shown in Fig. 1 demonstrate that f defined by Eq.(21) is well-represented by a linear function of the variable ζ, or $f \simeq \beta\zeta - 1$. The slope β depends on the temperature for which Eq.(20) was solved. In real time, this relationship is:

$$f(t) = Q(\sqrt{t} - \sqrt{t^*}) \tag{22}$$

where

$$Q = \frac{A_c S_M \sqrt{D_M} \sqrt{p^*_{O_2}}\, \beta}{\sqrt{\pi}\, V_p\, \rho_{UO_2}} \tag{23}$$

Because $f(0) = -1$, t^* and the parameter Q are related by:

$$t^* = Q^{-2} \tag{24}$$

5. Grain Boundary Diffusion and Reaction of Ruthenium with UO_{2-x}

During the interval $0 \leqslant t \leqslant t^*$, ruthenium diffuses in the UO_2 grain boundaries without reaction. For $t > t^*$, URu_3 formation provides a sink for the diffusing ruthenium and the diffusion equation is:

$$\frac{\partial \phi}{\partial t} = D_{gb} \frac{\partial^2 \phi}{\partial z^2} - J_{URu_3} \tag{25}$$

where ϕ is the concentration of ruthenium in the grain boundary at distance z from the source plane and D_{gb} is the grain boundary diffusivity. This equation applies to each side of the UO_{2-x}/URu_3 interface at the grain boundary. Because the amount of ruthenium physically dissolved in the grain

boundaries is quite small compared to the quantity which has reacted to form URu_3, the explicit time derivative on the left hand side of Eq. (25) can be neglected.

Using Eq. (16) for J_{URu_3}, the quasi-stationary form of Eq. (25) is:

$$D_{gb} \frac{d^2\phi}{dz^2} = k_R \left(1 - e^{-b\phi}\right) f(t) \tag{26}$$

The boundary conditions are:

$$\begin{aligned} \phi(0,t) &= \phi_s \\ \phi(\infty,t) &= 0 \end{aligned} \tag{27}$$

where ϕ_s is the solubility of metallic ruthenium (without URu_3 formation) in the grain boundaries of UO_2.

Equation (26) governs the system in the time interval $t^* \leq t \leq t_1$, during which the URu_3 layer thickness is less than δ_1 at all positions. At $t = t_1$, the layers at $z = 0$ reach the thickness at which oxygen transport stops and hence reaction ceases locally. For $t > t_1$, regions progressively further removed from the interface at $z = 0$ achieve layer thicknesses of δ_1. The function $z_1(t)$ denotes the distance from the interface over which the URu_3 layers are all of thickness δ_1 and no longer growing. By definition, $z_1(t_1) = 0$. For $t > t_1$, we have a two-zone diffusion problem. In the region $0 < z < z_1$, no reaction occurs, so the ruthenium diffusion equation is simply $d^2\phi/dz^2 = 0$ and the concentration varies linearly in z:

$$\phi = \phi_s + (d\phi/dz)z \tag{28}$$

This solution satisfies the first boundary condition Eq. (27). To simplify the analysis in the zone $z > z_1$, we define a dimensionless distance by:

$$\eta = (z - z_1) \left[\frac{bk_R f(t)}{D_{gb}}\right]^{1/2} \tag{29}$$

and a dimensionless concentration:

$$\theta = b\phi \tag{30}$$

which reduce Eq. (26) to:

$$\frac{d^2\theta}{d\eta^2} = 1 - e^{-\theta} \tag{31}$$

The boundary condition at $z = z_1$ (or $\eta = 0$) is obtained from Eq. (28):

$$\theta(0) = B + E(d\theta/d\eta)_{\eta=0} \tag{32}$$

and the final condition is:

$$\theta(\infty) = 0 \tag{33}$$

In Eq. (32),

$$B = b\phi_s \tag{34}$$

and

$$E = z_1 \left[\frac{bk_R f(t)}{D_{gb}}\right]^{1/2} \tag{35}$$

are constants, the latter a function of time.

Equations (31) - (33) can either be solved numerically, or by the accurate approximations described in the appendix.

6. URu_3 Layer Growth

Once the oxide is sufficiently substoichiometric to thermochemically permit formation of URu_3, this compound grows as a layer between urania grains. To supply its growth, uranium is provided by the adjacent grains (which thereby shrink slightly) and ruthenium is supplied by diffusion in the UO_{2-x}/URu_3

interface. As long as the layer thickness is less than the value which effectively blocks oxygen removal from the UO_2 grains, the oxygen produced by the reaction diffuses rapidly into the bulk urania and thence into the metal crucible. Since the reaction occurs on both sides of the URu_3 layer, the rate of change of the half-thickness of this layer is equal to the net rate of Eq.(6), given by Eq.(16), divided by the ruthenium density in URu_3:

$$\frac{\partial \delta}{\partial t} = \frac{k_R Q}{\rho_{URu_3}} \left(1 - e^{-b\phi}\right)\left(\sqrt{t} - \sqrt{t^*}\right)$$

As the layer thickness approaches the limiting value δ_1, the oxygen pressure p_{O_2} in Eq.(16), rises and eventually reaches $p^*_{O_2}$ when the encapsulating reaction product layer is thick enough to prevent all oxygen escape from the grain. Rather than attempt to model the exact kinetics of this aspect of the process, we require that $d\delta/dt$ vanish for $\delta \geq \delta_1$. For computational purposes, the growth law given by this equation is written in dimensionless terms:

$$\frac{\partial}{\partial \tau}(\delta/\delta_1) = \frac{1}{W}\left[1 - e^{-\theta(n,B,E)}\right](\sqrt{\tau} - 1) \tag{36}$$

where τ is the time relative to t^*:

$$\tau = t/t^* \tag{37}$$

and W is a dimensionless parameter:

$$W = \delta_1 Q^2 \rho_{URu_3}/k_R \tag{38}$$

The ruthenium concentration in the grain boundary, θ defined by Eq.(30),

was calculated in the preceding section as a function of the constant B of Eq. (34), the penetration distance variable of Eq. (29):

$$\eta = U(z - z_1)(\sqrt{\tau} - 1)^{\frac{1}{2}} \tag{39}$$

and the parameter of Eq. (35) which reflects the diffusional resistance of the nonreacting zone $0 < z < z_1$:

$$E = Uz_1(\sqrt{\tau} - 1)^{\frac{1}{2}} \tag{40}$$

The constant

$$U = (Bk_R/\phi_s D_{gb})^{\frac{1}{2}} \tag{41}$$

has the units of reciprocal length.

Growth prior to Saturation at the Interface

For the time interval $t^* < t < t_1$, the URu_3 layer thickness is everywhere less than δ_1 and layer growth is given by Eq. (36) with $z_1 = 0$ in Eqs. (39) and (40). Integration of Eq. (36) yields:

$$\frac{\delta}{\delta_1} = \frac{1}{W} \int_1^{\tau} \left[1 - e^{-\theta(\eta')}\right] (\sqrt{\tau'} - 1)\, d\tau' \tag{42}$$

Converting the variable of integration on the right hand side from τ' to $\eta' = Uz(\sqrt{\tau'} - 1)^{\frac{1}{2}}$ yields:

$$\frac{\delta}{\delta_1} = \frac{4}{W(Uz)^6} \int_0^{\eta} \left[1 - e^{-\theta(\eta')}\right] \eta'^3(\eta'^2 + U^2z^2)\, d\eta' \tag{43}$$

where $\eta = Uz\ (\sqrt{\tau} - 1)^{\frac{1}{2}}$.

The time $\tau_1 = t_1/t^*$ at which the terminal layer thickness δ_1 is just attained at $z = 0$ can be obtained by setting $\delta/\delta_1 = 1$ on the left hand side

of Eq. (43) and letting $\eta \to 0$ on the right hand side. The latter step reduces $\theta(\eta')$ to $\theta(0) = B$, so that the exponential term can be extracted from the integral. The time τ_1 is thus determined by solution of the equation:

$$2\tau_1^{3/2} - 3\tau_1 + 1 = 3W/(1-e^{-B}) \tag{44}$$

Layer Growth after Saturation at the Interface

When $\tau > \tau_1$, the saturated zone has moved away from the source plane ($z_1 > 0$). The τ-dependence of the right hand side of Eq. (36) is now partly due to the variation of θ with E and η, and hence with z_1. Because this last quantity is a numerical function of τ, Eq(36) must be integrated numerically at selected values of z. The integration is started at $\tau = \tau_1$ where δ/δ_1 is given by Eq. (43) at the appropriate value of z. At a time τ_1 determined by Eq(44) the blocking thickness δ_1 is reached at the origin (z = 0). At later times, the layer thickness δ_1 is reached at positions away from the interface. The moving front of reacted grains is located at position $z_1(t)$ for $t > t_1$, as shown in Fig. 2.

The rate of advance of the front dz_1/dt, is determined as follows. At a time t + dt, the moving front has advanced by a distance dz_1 and the thickness of the layer just ahead of the moving front has grown by an amount $d\delta$ given by:

$$d\delta = \left(\frac{\partial\delta}{\partial t}\right)_{z_1} dt$$

From the geometry shown in Fig. 2, we have:

$$d\delta = -\left(\frac{\partial \delta}{\partial z}\right)_{z_1} dz_1$$

Combining these two equations results in:

$$\frac{dz_1}{dt} = -\frac{(\partial\delta/\partial t)_{z_1}}{(\partial\delta/\partial z)_{z_1}} \tag{45}$$

In dimensionless terms, Eq(45) is:

$$\frac{dz_1}{d\tau} = -\left[\frac{\partial(\delta/\delta_1)}{\partial\tau}\right]_{z\to z_1} \Bigg/ \left[\frac{\partial(\delta/\delta_1)}{\partial z}\right]_{z\to z_1} \tag{46}$$

Using Equation (36) the numerator of Eq(46) is:

$$\left[\frac{\partial(\delta/\delta_1)}{\partial\tau}\right]_{z\to z_1} = \frac{1 - e^{-\theta(0)}}{W} \quad (\sqrt{\tau} - 1) \tag{47}$$

Defining a function:

$$V(\tau) = -\frac{W}{U}\left[\frac{\partial(\delta/\delta_1)}{\partial z}\right]_{z\to z_1} \tag{48}$$

Eq(46) becomes:

$$\frac{dz_1}{d\tau} = \frac{[1 - e^{-\theta(0)}]\ (\sqrt{\tau} - 1)}{U\,V(\tau)} \tag{49}$$

The function $V(\tau)$ is determined by integration of Eq(36) starting from $\tau = \tau_1$ at which time the relative layer thickness is denoted by $(\delta/\delta_1)_{\tau_1}$:

$$\frac{\delta}{\delta_1} - \left(\frac{\delta}{\delta_1}\right)_{\tau_1} = \frac{1}{W} \int_{\tau_1}^{\tau} \left[1 - e^{-\theta(\eta')}\right] (\sqrt{\tau'} - 1)\, d\tau' \tag{50}$$

Taking the derivative of this equation with respect to z [using Eq. (39) to accomplish the derivative of the integral on the right hand side] and expressing the result in terms of the $V(\tau)$ function of Eq(48) yields:

$$V(\tau) = -\frac{W}{U} \left[\frac{\partial(\delta/\delta_1)_{\tau_1}}{\partial z}\right]_{z\to z_1} + \int_{\tau_1}^{\tau} \left(-\frac{d\theta}{d\eta}\right)_0 e^{-\theta(0)} (\sqrt{\tau'} - 1)^{3/2} d\tau' \tag{51}$$

or:

$$\frac{dV}{d\tau} = (-d\theta/d\eta)_0\, e^{-\theta(0)} (\sqrt{\tau} - 1)^{3/2} \tag{52}$$

Eqs. (49) and (52) are solved simultaneously (and numerically) with the initial condition for the former given by:

$$z_1(\tau_1) = 0 \tag{53}$$

The initial condition for Eq. (52) is the first term on the right hand side of Eq. (51). This is obtained by setting $\tau = \tau_1$ in Eq. (42), taking the derivative with respect to z, and letting $z \to z_1$, which yields:

$$v(\tau_1) = 4(-d\theta/d\eta)_0\, e^{-\theta(0)} \left\{\frac{(\sqrt{\tau_1} - 1)^{7/2}}{7} + \frac{(\sqrt{\tau_1} - 1)^{5/2}}{5}\right\} \tag{54}$$

The values of the function θ and its derivative at $\eta = 0$ are obtained from the results of section 5. Once z_1 has been determined as a function of

τ, Eq. (36) can be integrated numerically to obtain the growth of the relative layer thickness at various values of z. The constants B, U, and W have to be specified for these computations. Figure 3 displays the layer thickness profiles for several dimensionless times.

7. Fitting Theory and Experiment

In the previous section, the method of calculating the distribution in z of the relative URu_3 layer thickness δ/δ_1 at dimensionless time τ was described. This computation requires specification of the constants B[Eq(34)], U[Eq(41)], and W[Eq(38)]. In order to compare theory with experiment, the dimensionless time τ must be related to real time, which is accomplished by combining Eqs(24) and (37):

$$\tau = Q^2 t \tag{55}$$

where Q is the parameter defined by Eq. (23). Finally, the relative layer thickness is related to the measured ruthenium-to-uranium ratio, C, by:

$$C = C_o(\delta/\delta_1) \tag{56}$$

where C_o is given by Eq(3).

Thus, prediction of the variation of C with z at a fixed time and known temperature requires specification of 5 constants, namely B, U, W, Q, and C_o. Since each of these parameters has an Arrhenius-type temperature dependence, correlation of data taken over a range of temperature involves 10 fitting parameters.

The data reported in Ref. 1 pertain to isothermal annealing of specimen assemblies consisting of a layer of ruthenium powder (or a massive disk) clamped between a UO_2 pellet and a UO_2 wafer. Some experiments

contained two assemblies, which provides an estimate of the reproducibility of the phenomenon. The measured ruthenium concentration distributions were symmetric about the source plane. Figures 4a - 4f show the data for experiments in which only tungsten was in contact with the specimens. The curves in Fig. 4 are those produced by the model calculations described above in which values of the five parameters were chosen to provide the best fit to the data of each temperature. Comparable fitting of theory to the experiments in which molybdenum contacted the specimen is shown in Fig. 5. In this case, the scarcity of data permitted determination only of ranges of the model parameters at each temperature, so the theoretical predictions are plotted as bands in Fig. 5.

The five parameters determined by the data-fitting process are shown in Fig. 6. The lines represent the best fits to the parameters obtained from the experiments utilizing tungsten hardware. Each of the five parameters shows satisfactory Arrhenius behavior with the activations energies listed on the graphs.

Assuming that the quantity b (which relates the fractional areal coverage of the grain boundary by ruthenium patches to the average ruthenium concentration) is temperature-independent, the 125 kcal/mole activation energy of the parameter B(Eq. (34)) represents the enthalpy of solution of ruthenium in the UO_2 grain boundaries (without reaction to form URu_3).

The oxide reduction parameter Q is the only one of the five which explicitly contains properties of the refractory metal contacting the specimen. The enthalpy associated with the product $\sqrt{p^*_{O_2}}\ \beta$ in Eq. (23) is $\sim$40 kcal/mole. Therefore to achieve the activation energy of -48 kcal/mole listed on the Q-graph in Fig. 6, the permeability of tungsten

to oxygen must have an activation energy of -88 kcal/mole. Because the activation energy of D_M is certainly positive, solution of oxygen in tungsten must be endothermic by more than 88 kcal/mole. Although the solubility of oxygen in tungsten has not been measured, Srivastava and Seigle have determined the terminal solubility of oxygen in molybdenum(8). Their data, when combined with the standard free energy of formation of MoO_2, show that solution of O_2 in [(i.e., the enthalpy associated with S_M of Eq(17)] is endothermic by 11 kcal/mole.

The activation energy of 170 kcal/mole of C_o translates, according to Eq.(3), to the temperature-dependence of the blocking layer thickness δ_1. As discussed in section 2, δ_1 increases with temperature as does the permeability of URu_3 to oxygen. The large positive activation energy of this quantity is expected, and indicates exothermic solution of oxygen in the intermetallic compound.

The parameters W and U defined by Eqs.(38) and (41) respectively are composite quantities. However, by combining the definitions of the five model parameters, the activations energies of grain boundary diffusion of ruthenium in UO_2 and of the chemical reaction rate constant for URu_3 formation can be obtained. These are:

$$E_{D_{gb}} = E_{C_o} + 2E_Q - E_W - 2E_U$$

and

$$E_{k_R} = E_{C_o} + 2E_Q - E_W$$

Using the activation energies given in Fig. 6 in the right hand sides of these formulas gives $E_{D_{gb}}$ = 158 kcal/mole and E_{k_R} = 148 kcal/mole. The latter value appears to be reasonable for a chemical reaction between two refractory solids (i.e., Ru and UO_2) but the former seems high for grain boundary diffusion, at least by comparison to metals in metals.

The model parameters deduced from the anneals with molybdenum fittings are also plotted in Fig. 6. The Q-parameter is ∿25% larger for the specimens in contact with molybdenum than those in contact with tungsten. This difference implies a correspondingly larger permeability of the former refractory metal for oxygen. The C_o values shown in the last panel of Fig. 6 are unaffected by the type of container. However, the other parameters, B, W, and U, are different for the two container metals. As can be seen from Fig. 6, the major effect of changing the metal fittings from tungsten to molybdenum is to reduce the parameter U by a factor of ∿2, which, according to Eq. (41), can be attributed to a factor of four increase of D_{gb}. Although the parameters B, W, and U do not explicity contain properties of the container metal, impurities from the latter could enter the urania and thereby affect its interaction with ruthenium. Carbon is a possible impurity since it is more likely to be present in the arc-cast molybdenum from which the fittings were fabricated than in the CVD tungsten parts. An alternative explanation of the sensitivity to container metal may be the slightly more vigorous oxygen-gettering action of molybdenum. The urania reduction rates calculated by the method described in Section 4 for the Q-values shown in Fig. 6 imply O/U ratios at the end of the lowest and highest temperature anneals in tungsten of 1.99 and 1.98, respectively. The slightly larger value of Q in the experiments utilizing

molybdenum fittings results in somewhat more extensive oxide reduction. Such reduction is accompanied by production of anion vacancies, which could enhance the mobility of ruthenium in the grain boundaries and result in the larger grain for boundary diffusivity for molybdenum implied by the U-plot in Fig. 6.

8. Ruthenium Transport in a Temperature Gradient

Reference 1 reported the results of ruthenium spreading from a source plane at 2500 K into UO_2 subjected to a temperature gradient of 1400 K/cm. In this experiment, the wafer side of the UO_2 specimen was hot and the pellet side was cold. Considerable migration of ruthenium into the hot wafer was observed but very little penetration of the cooler UO_2 pellet occurred. The hot portions of the specimen were contained in a tungsten crucible. The mobility of ruthenium in a thermal gradient differs from that in an isothermal anneal for the following reasons. First, the properties of the interaction, particularly the diffusivity D_{gb}, the reaction rate coefficient k_R, and the effective solubility C_o, increase rapidly with temperature. Second, ruthenium migration by ordinary grain boundary diffusion may be aided or hindered by thermal diffusion characterized by a heat of transport Q^*_{Ru}. Third, the UO_2 wafer on the hot side of the source plane is isolated from the cooler pellet by the ruthenium layer. As a result, the wafer side of the specimen is probably more highly reduced than the pellet side. Finally, the presence of a temperature gradient in the UO_2 causes oxygen redistribution characterized by a heat of transport Q^*_O. Oxygen redistribution is superimposed on the reduction process and as a result, the critical oxygen pressure for URu_3 formation occurs at times which are position-dependent.

Most of the ruthenium spreading data in the temperature gradient test was obtained for the wafer (hot) side of the specimen, and only these data will be modeled. The first requirement is to estimate the rate of reduction of the urania on the hot side of the source plane. Rather than attempt to model the reduction process in a variable temperature field, we assume that the O/U ratio of the hot side of the specimen is reduced at a rate characteristic of the average temperature of the wafer, which is ∿2570 K. Next, we assume that oxygen redistribution follows the Arrhenius form:

$$2 - O/U = K\exp(-Q_O^*/RT) \tag{57}$$

where K is a constant obtained by normalizing the oxygen distribution to the instantaneous average O/U ratio over the 1 mm thickness of the wafer on the hot side of the ruthenium source plane. The heat of transport of oxygen in hypostoichiometric urania is taken as -30 kcal/mole(9,10).

Having established the O/U ratio as a function of t and z in the UO_2 wafer, the time- and position-dependence of the reaction rate factor f of Eq(21) can be computed. A reasonably faithful approximation to this function is found to be:

$$f(t,z) \simeq e^{-az}\left[\sqrt{\frac{t}{t^*(0)}} - \sqrt{\frac{t^*(z)}{t^*(0)}}\right] \tag{58}$$

where a is a numerical constant and $t^*(z)$ is the time at which p_{O_2} reaches $p_{O_2}^*$ (so that URu_3 formation can begin) at a distance z from the source plane. The ratio $t^*(z)/t^*(0)$ was found to be very closely represented by a linear function of z. Because of the effect of the temperature gradient on the oxygen potential of UO_{2-x}, the coolest zone first achieves the critical O/U for URu_3 formation - that is, $t^*(z)$ increases with z.

Because the mechanism of ruthenium spreading in UO_2 is presumed to be the same in the thermal gradient as in the isothermal anneals, ruthenium diffusion and reaction with UO_2 is governed by:

$$- \frac{dj}{dz} = k_R(1 - e^{-b\phi})f(z,t) \tag{59}$$

where the ruthenium flux j in the UO_2 grain boundaries includes contributions from ordinary diffusion and thermal diffusion:

$$j = - D_{gb}\left[\frac{d\phi}{dz} + \phi\left(\frac{Q^*_{Ru}}{RT}\right) \frac{1}{T} \frac{dT}{dz}\right] \tag{60}$$

Equation (59) applies to the zone $z_1 \leq z \leq z_2$ and to the time interval $t^*(z) \leq t \leq t_f$, where t_f is the time of the thermal gradient experiment. As in the treatment of the isothermal anneals, z_1 is the time-dependent position of the reaction front. In the zone $0 \leq z \leq z_1$, the reaction product URu_3 has grown to layer thicknesses (δ_1) sufficient to prevent removal of reaction product oxygen by absorption by the refractory metal sink. At this location the concentration ϕ and the gradient $d\phi/dz$ are related by Eq(28), just as in the isothermal case. The other limit of applicability of Eq(59) is the position at which the critical O/U ratio for URu_3 is just achieved, which is determined by solution of:

$$t = t^*(z_2) \tag{61}$$

the function $t^*(z)$ having been previously determined by modeling of the wafer reduction rate and t being the current time. For $z > z_2$, no reaction between ruthenium and urania can occur, because the urania is still insufficiently reduced to thermodynamically permit URu_3 formation. Because the grain boundaries of UO_2 have been assumed to have negligible

capacity for ruthenium in the absence of the reaction which forms the intermetallic compound, we take the second boundary condition to be one of zero flux into the nonreactive zone beyond z_2:

$$j(z=z_2) = 0 \tag{62}$$

Substituting Eqs. (58) and (60) into Eq. (59) and converting the diffusion equation and its boundary conditions to dimensionless form yields:

$$\frac{d}{dZ}\left[F_{gb}(Z)\left(\frac{d\theta}{dZ} + S\theta\right)\right] = F_R(Z)e^{-AZ}\left[\sqrt{\tau} - \sqrt{\frac{t^*(Z)}{t^*(0)}}\right] \tag{63}$$

$$F_{gb}(Z) = \exp\left[-\frac{E_{D_{gb}}}{RT_s}\left(\frac{T_s}{T} - 1\right)\right] \tag{64}$$

$$F_R(Z) = \exp\left[-\frac{E_{k_R}}{RT_s}\left(\frac{T_s}{T} - 1\right)\right] \tag{65}$$

$$A = a/U_s \tag{66}$$

$$Z = zU_s \tag{67}$$

$$U_s = \left(\frac{bk_{Rs}}{D_{gbs}}\right)^{\frac{1}{2}} \tag{68}$$

$$S = \left(\frac{Q^*_{Ru}}{RT_s}\right)\frac{1}{T_s}\frac{dT}{dz}\frac{1}{U_s} \tag{69}$$

$$\tau = t/t^*(0) \tag{70}$$

and $\theta = b\phi$. The temperature at the source plane is denoted by T_s and the subscript s indicates quantities evaluated at this temperature.

The boundary condition at the outer edge of the ruthenium saturated zone is:

$$\theta(Z=Z_1) = B_s + Z_1 \left(\frac{d\theta}{dZ}\right)_{Z_1} \tag{71}$$

while Eqs. (60) and (62) yield:

$$\left(\frac{d\theta}{dZ}\right)_{Z_2} + S\theta(Z=Z_2) = 0 \tag{72}$$

Z_2 being determined from Eq. (61)

Eq. (63) is solved numerically with the boundary conditions of Eqs. (71) and (72) to determine the concentration profile $\theta(Z,\tau)$. At each location away from the source plane, the rate of growth of the URu_3 layer is given by:

$$\frac{d\delta}{dt} = \frac{k_R}{\rho_{URu_3}} (1 - e^{-b\phi}) f(t,z) \tag{73}$$

Converting this equation to dimensionless terms and allowing for the temperature dependence of the model parameters yields:

$$\frac{d(\delta/\delta_1)}{d\tau} = \frac{1}{W_s} \frac{F_R(Z)e^{-AZ}}{F_{C_o}(Z)} (1 - e^{-\theta}) \left[\sqrt{\tau} - \sqrt{\frac{t^*(Z)}{t^*(0)}}\right] \tag{74}$$

where

$$W_s = \frac{\delta_{1s}\rho_{URu_3}}{k_{Rs}\, t^*(0)} \tag{75}$$

Eq. (74) is to be integrated for various values of Z for time intervals from $\tau = t^*(Z)/t^*(0)$ to the final anneal time, $\tau = t_f/t^*(0)$. δ_{1s} in Eq. (75) is the value of the blocking layer thickness at the source plane (Z = 0). Both δ_1 and C_o vary with position according to:

$$\frac{\delta_1}{\delta_{1s}} = \frac{C_o}{(C_o)_s} = F_{C_o}(Z) \tag{76}$$

where

$$F_{C_o}(Z) = \exp\left[-\frac{E_{C_o}}{RT_s}\left(\frac{T_s}{T} - 1\right)\right] \tag{77}$$

Having integrated Eq. (63) with respect to Z at several specified values of τ and used this result to integrate Eq. (74) with respect to τ at fixed values of Z, the distributions of the relative layer thicknesses δ/δ_1 at various distances from the source plane at the time corresponding to the termination of the thermal gradient anneal are calculated. From this result, the ruthenium-to-uranium ratio is computed from:

$$C = (C_o)_s(\delta/\delta_1)F_{C_o}(Z) \tag{78}$$

The calculation requires prior specification of 8 parameters, viz the 2500 K values of C_o, B, U and W, the activation energies $E_{D_{gb}}$, E_{k_R}, and E_{C_o} and the ruthenium Soret parameter S of Eq. (69). The first 7 of these have already been determined from the analysis of the isothermal anneal. However, independent values of the same parameters are selected to provide the best fit to the experimental ruthenium distribution following the thermal gradient anneal. The theoretical curves are compared to the data in Fig. 7 for heats of transport of ruthenium of -100, 0 and 100 kcal/mole. The parameters so determined are listed in Table 1 where they are compared to the values used to fit the isothermal anneal data. In general, the parameter values which provide the best fit to the thermal gradient data are close to those found from the isothermal spreading data, the sole exception being U_s. This parameter is three times smaller in the thermal gradient experiment than in the isothermal tests. The theoretical curves in Fig. 7 reproduce, albeit in exaggerated form, the observed maximum ruthenium concentration which

occurs between 200 and 400 μm from the source plane. The concentration maximum occurs because the URu_3 layer reaches the terminal thickness throughout the first 100 μm. Because δ_1 increases with temperature, the observed ruthenium concentration at first increases with distance from the source plane. For distances beyond 100 μm, the rate of URu_3 growth is limited by ruthenium supply along the grain boundary, and the concentration decreases to nearly zero at a distance of one millimeter from the source plane.

The heat of transport of ruthenium in the grain boundaries of UO_2 has only a modest effect on the spreading. It can be concluded that the observed ruthenium distribution in the thermal gradient test is not due to a true thermal diffusion effect; rather it is simply a result of the temperature-dependence of various physico-chemical properties of the Ru/UO_2 system, particularly the thickness of the URu_3 layer in the grain boundary at which the reaction is choked by its reaction product (oxygen) which can no longer be removed by the refractory metal sink.

Table 1. Interaction parameters deduced from ruthenium spreading in UO_2 in a temperature gradient and under isothermal conditions

	Parameter	Value: Isothermal	Value: Temperature Gradient
at 2500 K	B	4.4	4.3
	U	0.018	0.006
	W	6.7	4.2
	$C_o \times 10^4$	170	130
kcal/mole	$E_{D_{gb}}$	158	172
	E_{k_R}	148	148
	E_{C_o}	170	175

9. Conclusions

The proposed ruthenium-UO_2 interaction model is based upon solution, diffusion and reaction of the metal in the grain boundaries of the hypo-stoichiometric ceramic. There is virtually no interaction at temperatures below ∿2300 K but extensive reaction and spreading is observed at 2570 K. To match this highly temperature-sensitive behavior, the parameters of the model exhibit large activation energies.

The model is applied to ruthenium transport from a source plane in UO_2 in both isothermal and temperature gradient tests. Good agreement with the data is obtained in both cases. In particular, the observed maximum in the ruthenium concentration distribution away from the source plane is successfully reproduced by the model.

The model is based on a static microsctructure; it does not treat the extensive grain growth in UO_2 which is observed in the tests and which may assist ruthenium transport.

Acknowledgement

This work was supported by the Director, Office of Energy Research, Office of Basic Energy Sciences, Materials Sciences Division of the U.S. Department of Energy under contract #W-7405-ENG-48.

REFERENCES

1. R.L. Yang and D.R. Olander, Nucl. Technol., to be published.
2. A.H. Booth, AECL Report CRDC-721 (1957)
3. D.G. Hurst, AECL Report AECL-1550 (1962)
4. H.S. Levine and C.J. MacCallum, J. Appl. Phys. 31, 595 (1960)
5. R.P. Agarwala et al., J. Nucl. Mater. 36, 41 (1970)
6. R.B. Snyder, K. Natesan and T.F. Kassner, J. Nucl. Mater. 50, 259 (1974)
7. D.R. Olander, J. Nucl. Mater., 96, 243 (1981)
8. S.C. Srivastava and L.L. Seigle, Met. Trans., 5, 49 (1974)
9. M. Bober and G. Schumacher, Advan. Nucl. Sci. Technol. 7, 121 (1973)
10. E.A. Aitken, M.G. Adamson, S.K. Evans and T.E. Ludlow, General Electric Company Report GEAP-12254 (1970)

APPENDIX - Approximate Solution of the Grain Boundary Diffusion-Reaction Equation

Accurate approximate solutions of Eq(31) for the case E = 0 are developed below. The corresponding results for nonzero E are then given without derivation.

If the parameter B is small (i.e., < 1), θ must be < 1 because of the boundary conditions. Therefore, the right hand side of Eq. (31) is reduced to $1 - e^{-\theta} \simeq \theta$, and the solution to Eq(31) which satisfies Eqs. (32) and (33) is:

$$\theta = Be^{-\eta} \tag{A-1}$$

Fig. A-1 shows this approximation and the numerical results for B = 0.2 and E = 0.

Even when B >> 1, the approximation $1 - e^{-\theta} \simeq \theta$ must apply at a sufficiently large distance because of the boundary condition of Eq(33). Therefore, for large η, the solution must approach

$$\theta_L = Ke^{-\eta} \tag{A-2}$$

no matter what value of B is involved. Here K is a constant to be determined.

If B is large <u>and</u> $\eta \to 0$, the $e^{-\theta}$ term in Eq(31) is negligible compared to unity and the zeroth order, short-distance approximation to the exact solution is:

$$\theta_s^\circ = \tfrac{1}{2}\eta^2 - M_1\eta + B \tag{A-3}$$

which satisfies Eq(32) (for E = 0).

The unknowns K and M_1 are determined by matching the θ_L and θ_s° functions and their first and second derivatives at a distance η_1. The condition:

$$\left(\frac{d^2\theta_s^\circ}{d\eta^2}\right)_{\eta_1} = \left(\frac{d^2\theta_L}{d\eta^2}\right)_{\eta_1} \tag{A-4}$$

yields:

$$1 = Ke^{-\eta_1}$$

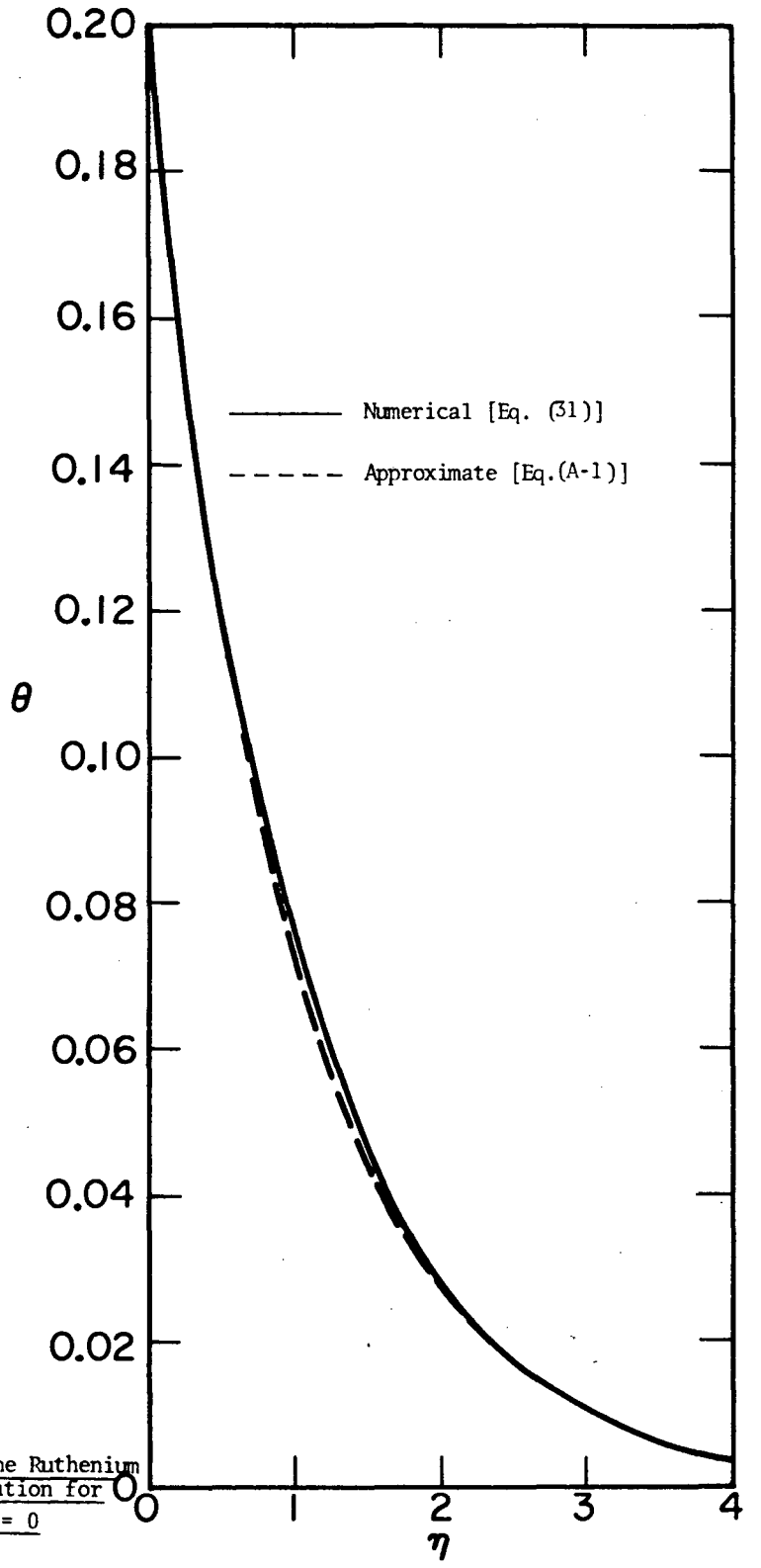

FIG.A-1 Solution of the Ruthenium Diffusion Equation for B = 0.2 and E = 0

The matching condition:

$$\left(\frac{d\theta_s^\circ}{d\eta}\right)_{\eta_1} = \left(\frac{d\theta_L}{d\eta}\right)_{\eta_1} \tag{A-5}$$

provides:

$$- M_1 + \eta_1 = - Ke^{-\eta_1}$$

and the final condition:

$$\theta_s^\circ(\eta_1) = \theta_L(\eta_1)$$

gives:

$$\tfrac{1}{2}\eta_1^2 - M_1\eta_1 + B = Ke^{-\eta_1} \tag{A-6}$$

The parameters determined by solving Eq(A4) - (A6) are:

$$M_1 = (2B - 1)^{\frac{1}{2}} \tag{A-7}$$

$$\eta_1 = M_1 - 1 \tag{A-8}$$

$$K = \exp(\eta_1) \tag{A-9}$$

Comparison of this solution (i.e., $\theta = \theta_s^\circ$ for $\eta < \eta_1$ and $\theta = \theta_L$ for $\eta > \eta_1$) with the exact numerical solution shows the former to be a poor approximation even for large values of the parameter B. An improved short-distance approximation can be obtained by approximating $e^{-\theta}$ in Eq.(31) by $e^{-\theta_s^\circ}$ instead of by zero, where θ_s° is given by Eq.(A3). We then must integrate:

$$\frac{d^2\theta_s}{d\eta^2} = 1 - \exp(-\tfrac{1}{2}\eta^2 + M_1\eta - B) \tag{A-10}$$

where M_1 is given by Eq (A7). Integrating this equation yields:

$$\theta_s = \tfrac{1}{2}\eta^2 + N_1\eta + N_2 - \sqrt{\pi}\exp(-B + M_1^2/2)\left\{\frac{\exp -\left(\frac{\eta - M_1}{\sqrt{2}}\right)^2}{\sqrt{\pi}} - \left(\frac{\eta - M_1}{\sqrt{2}}\right)\operatorname{erfc}\left(\frac{\eta - M_1}{\sqrt{2}}\right)\right\} \quad \text{(A-11)}$$

where N_2 is determined by applying Eq(32) (with $E = 0$):

$$N_2 = B + e^{-B} + \sqrt{\frac{\pi}{2}}\ M_1 \exp(-B + M_1^2/2)\ \operatorname{erfc}(-M_1\sqrt{2}) \quad \text{(A-12)}$$

N_1 and K are constants to be determined by application of the matching conditions of Eqs(A4) - (A6) involving θ_s instead of θ_s°, which yields:

$$1 - \exp(-\tfrac{1}{2}\eta_1^2 + M_1\eta_1 - B) = Ke^{-\eta_1} \quad \text{(A-13)}$$

$$\eta_1 + N_1 + \sqrt{\frac{\pi}{2}}\ \exp(-B + M_1^2/2)\ \operatorname{erfc}\left(\frac{\eta_1 - M_1}{\sqrt{2}}\right) = -\ Ke^{-\eta_1} \quad \text{(A-14)}$$

$$\tfrac{1}{2}\eta_1^2 + N_1\eta_1 + N_2 - \sqrt{\pi}\ \exp(-B + M_1^2/2)\left\{\frac{\exp -\left(\frac{\eta - M_1}{\sqrt{2}}\right)^2}{\sqrt{\pi}} - \left(\frac{\eta_1 - M_1}{\sqrt{2}}\right)\operatorname{erfc}\left(\frac{\eta_1 - M_1}{\sqrt{2}}\right)\right\}$$

$$= Ke^{-\eta_1} \quad \text{(A-15)}$$

which are solved for N_1, K, and η_1. This improved approximation (i.e., Eq(A11) for $\eta < \eta_1$ and Eq(A2) for $\eta > \eta_1$) provides an excellent fit to the exact numerical solutions of Eq(31) for $B > 1$ (see Fig. A-2)

For the case $E \neq 0$, the analysis results in:

<u>Small B</u>:

$$\theta = \frac{B}{1 + E}\ e^{-\eta} \quad \text{(A-16)}$$

<u>Large B</u>:

Eq(A2) still applies at large η. The zeroth order approximation for small distances is:

$$\theta_s^\circ = \tfrac{1}{2}\eta^2 - (\eta + E)M_1 + B \quad \text{(A-17)}$$

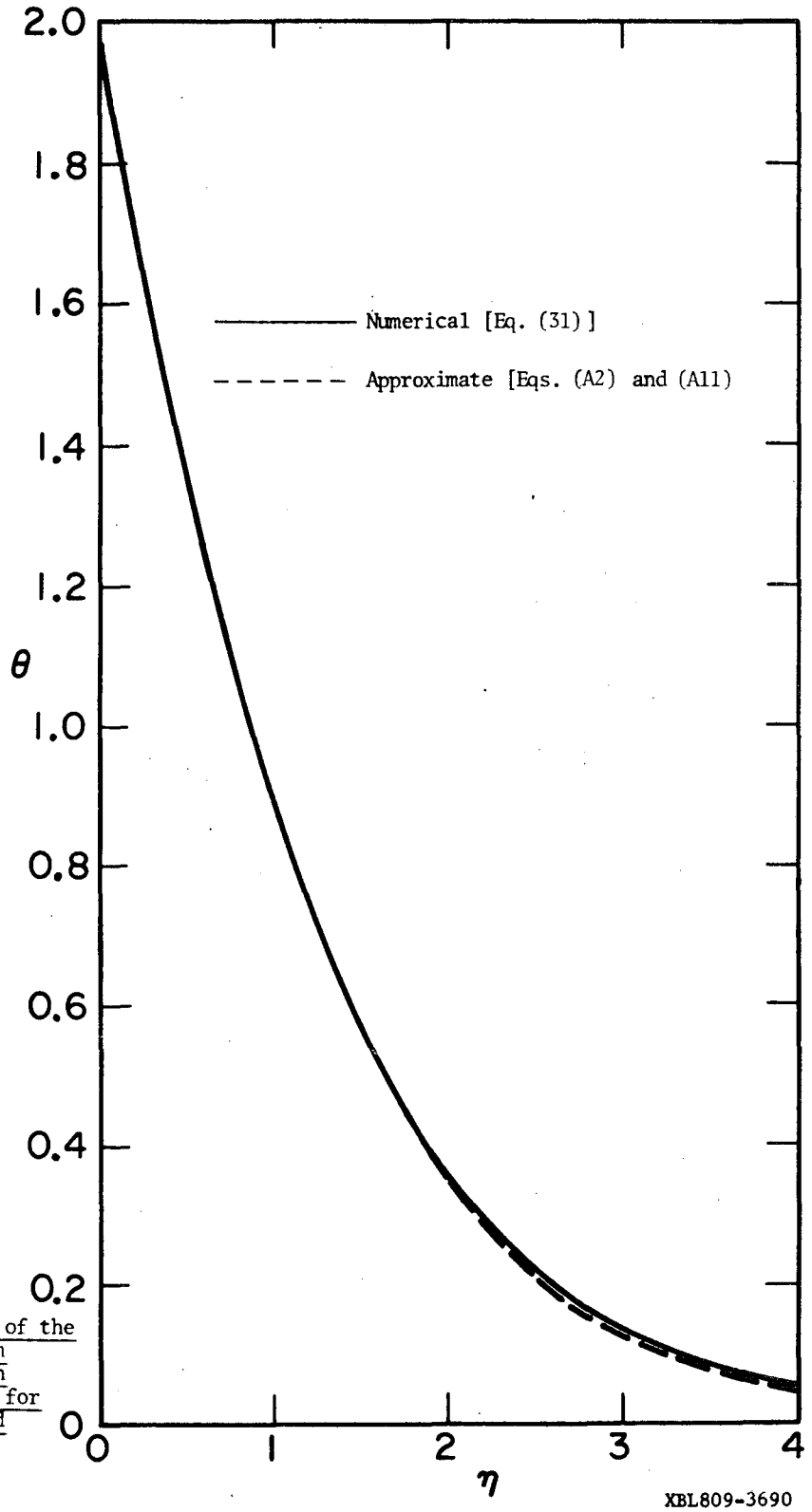

Fig. A2 Solution of the Ruthenium Diffusion Equation for B = 2 and E = 0

for which:

$$M_1 = \left\{2[B - (1+E)] + (1+E)^2\right\}^{\frac{1}{2}} - E \qquad \text{(A-18)}$$

Eqs (A8) and (A9) are valid for nonzero E. The first order approximation is:

$$\theta_s = \tfrac{1}{2}\eta^2 + N_1\ (\eta+E) + N_2 - \sqrt{\pi}\ \exp(-B+M_1E+M_1^2/2)\left\{\frac{\exp - \left(\frac{\eta-M_1}{\sqrt{2}}\right)^2}{\sqrt{\pi}} - \left(\frac{\eta-M_1}{\sqrt{2}}\right)\operatorname{erfc}\left(\frac{\eta-M_1}{\sqrt{2}}\right)\right\} \qquad \text{(A-19)}$$

where

$$N_2 = B + \exp(-B+M_1E) + \sqrt{\frac{\pi}{2}}\ \exp(-B+M_1E+M_1^2/2)\,(M_1+E)\ \operatorname{erfc}\ (-M_1/\sqrt{2}) \qquad \text{(A-20)}$$

The constants K, N_1 and η_1 are determined from equations similar to Eqs (A13)-(A15) except that a term M_1E is added to the arguments of all exponentials on the left hand sides except the one in the brackets of Eq (A15) Figure A-3 shows the effect of E on the ruthenium distribution for B = 10.

For small B(<1), Eq. (A16) gives:

$$\theta(0) = (-d\theta/d\eta)_0 = B/(1 + E) \qquad \text{(A-21)}$$

At large B(>1), Eq (A19) gives:

$$\theta(0) = N_1E + N_2 - \sqrt{\pi}\ \exp(-B+M_1E+M_1^2/2)\left[\frac{\exp(-M_1^2/2)}{\sqrt{\pi}} + \frac{M_1}{\sqrt{2}}\operatorname{erfc}(-\frac{M_1}{\sqrt{2}})\right] \qquad \text{(A-22)}$$

$$(-d\theta/d\eta)_0 = -N_1 - \frac{\sqrt{\pi}}{2}\ \exp\ (-B+M_1E+M_1^2/2)\ \operatorname{erfc}\ (-M_1/\sqrt{2}) \qquad \text{(A-23)}$$

where M_1, N_1, and N_2 are the functions of B and E obtained earlier.

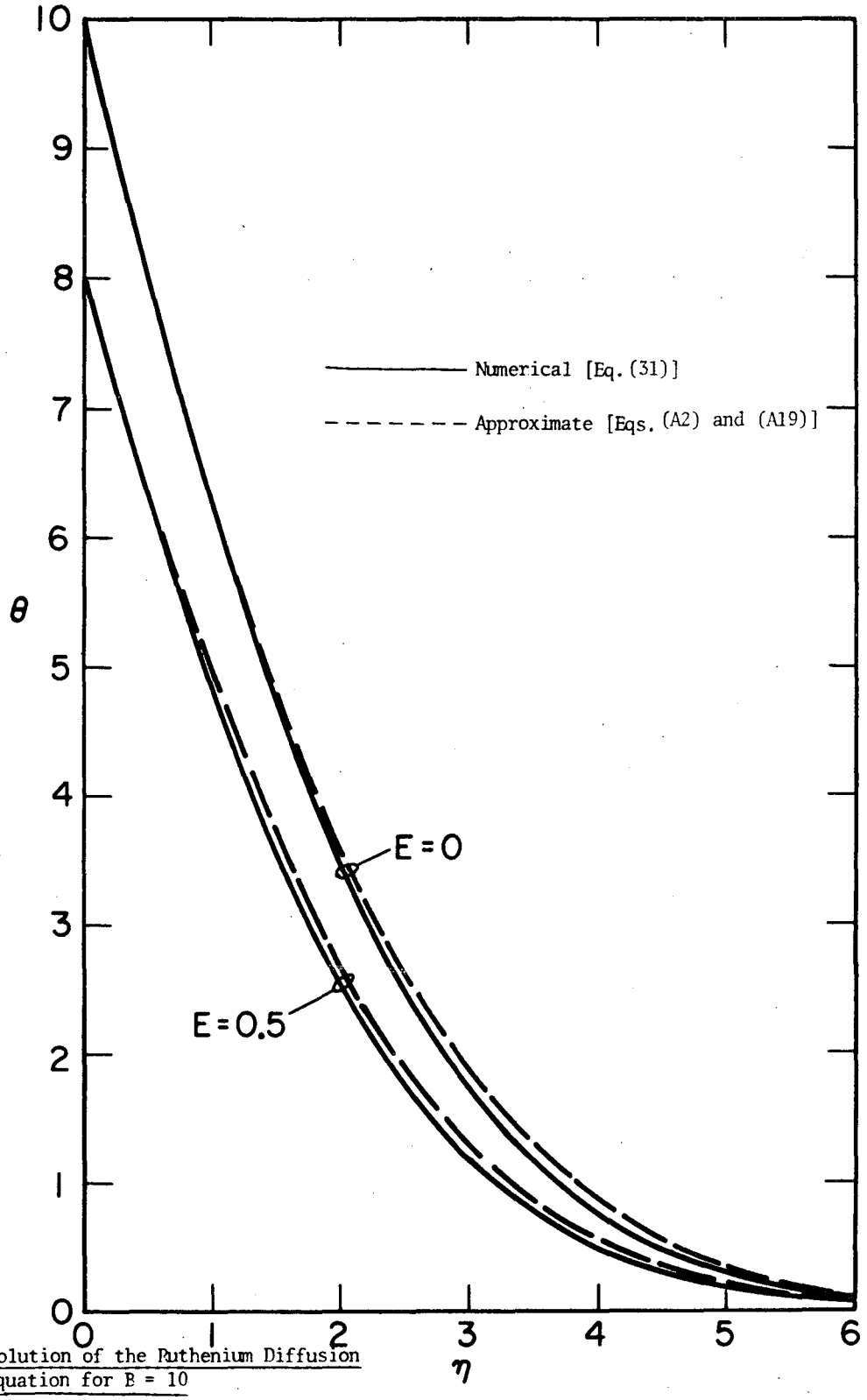

FIG. A3 Solution of the Ruthenium Diffusion Equation for B = 10

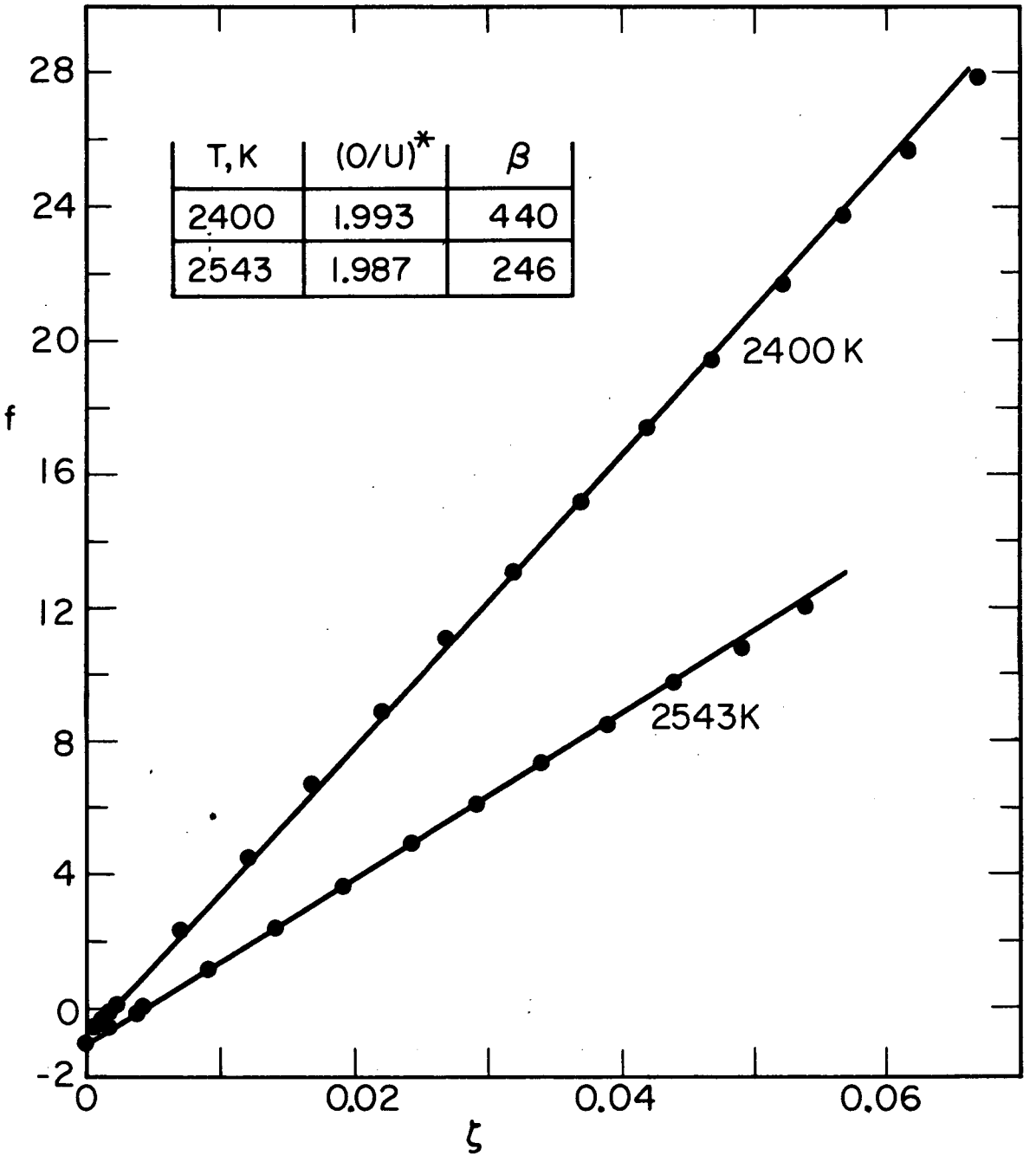

XBL809-3694

FIG. 1 Function describing reduction of urania by an oxygen-absorbing metal (points are numerically computed)

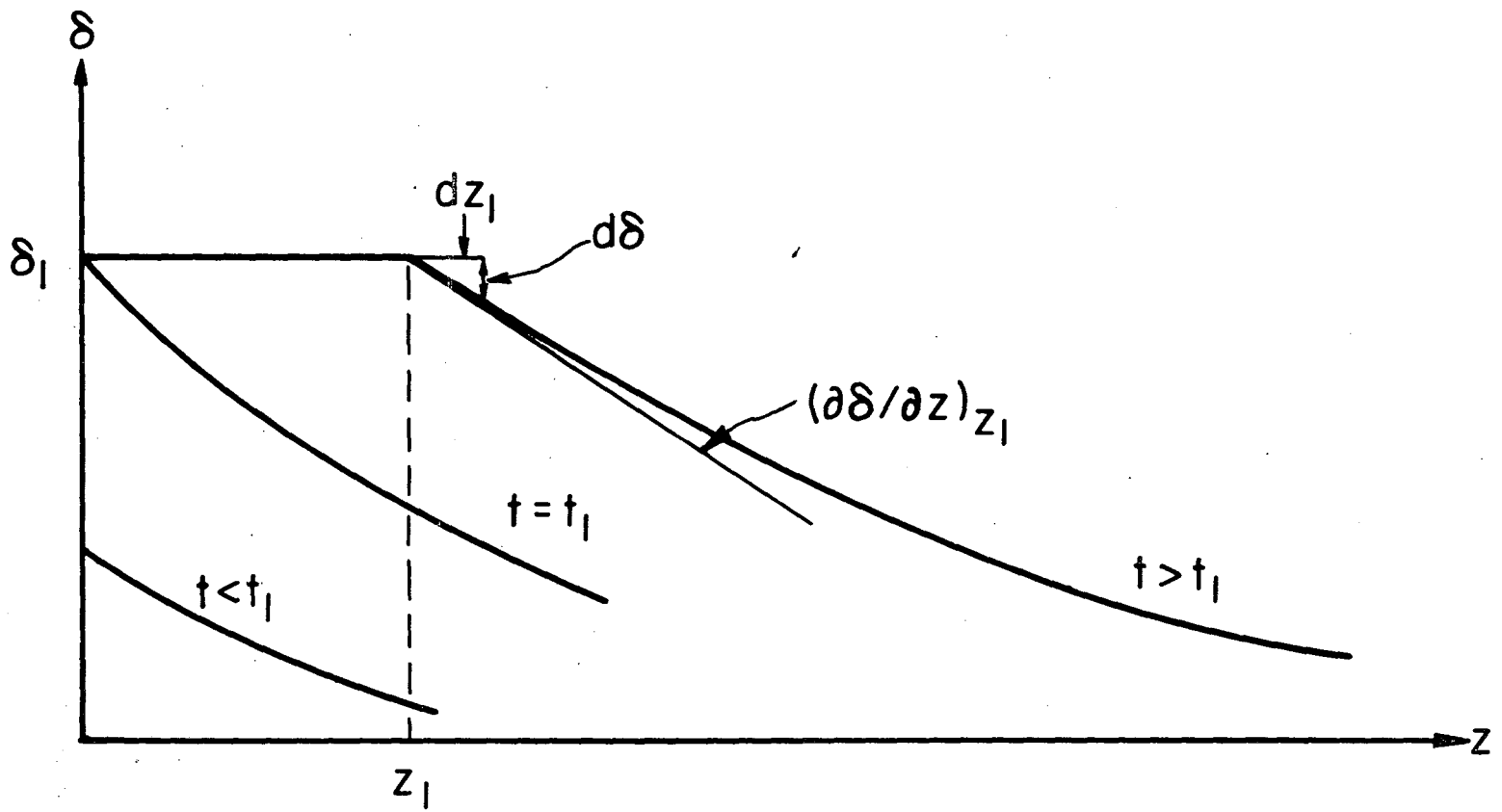

XBL812-3649

FIG 2 Diagram for calculating the rate of advance of the ruthenium-saturated front

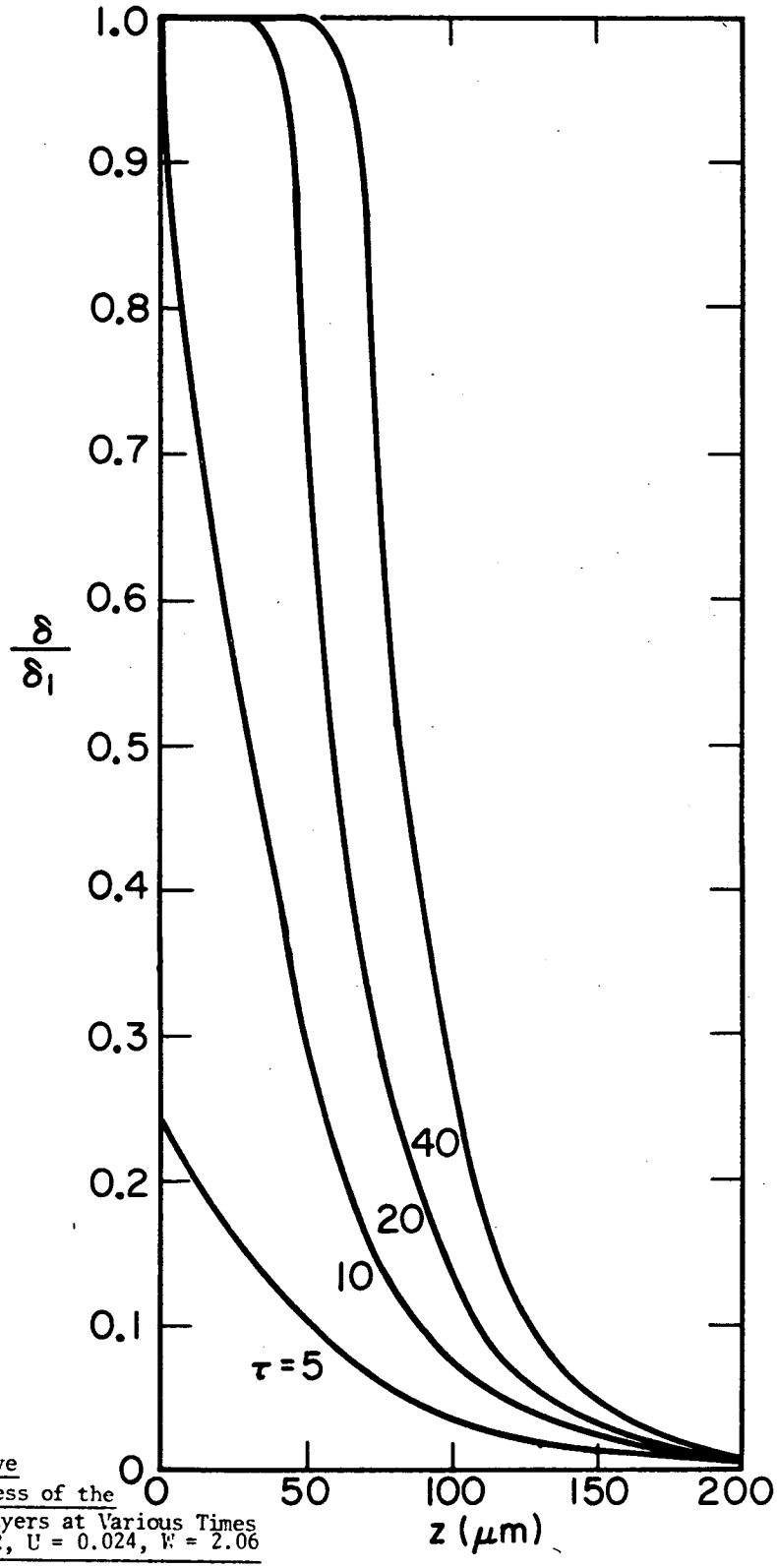

FIG. 3 Relative Thickness of the URu3 Layers at Various Times B = 0.2, U = 0.024, W = 2.06

XBL809-3693

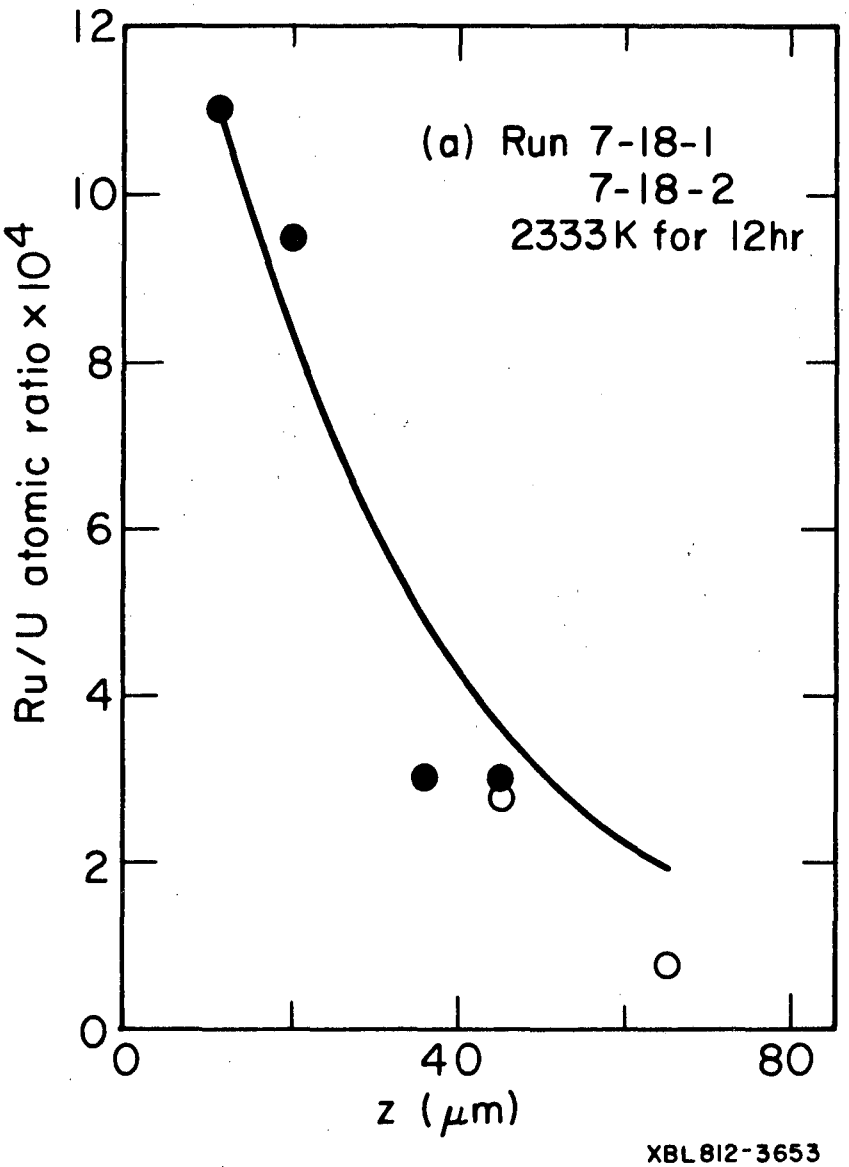

FIG 4(a) - (f) Ruthenium distributions following isothermal anneals with tungsten fittings; ○ pellet side of source plane; ● wafer side of source plane; ——— model fit to data

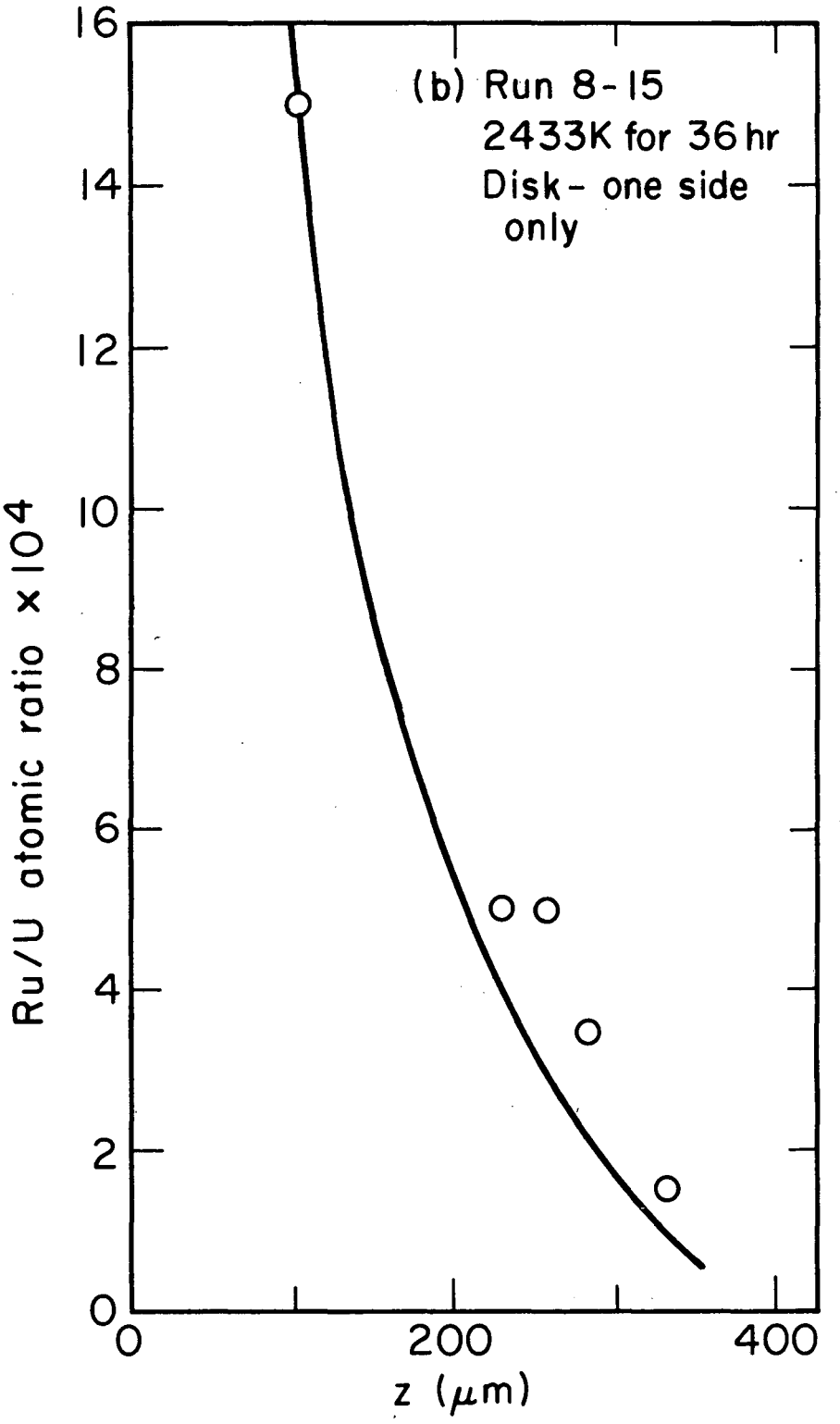
(b) Run 8-15
2433K for 36 hr
Disk - one side only
Ru/U atomic ratio x 10^4
z (μm)
0
2
4
6
8
10
12
14
16
0
200
400
XBL 812-3656

FIG 4b

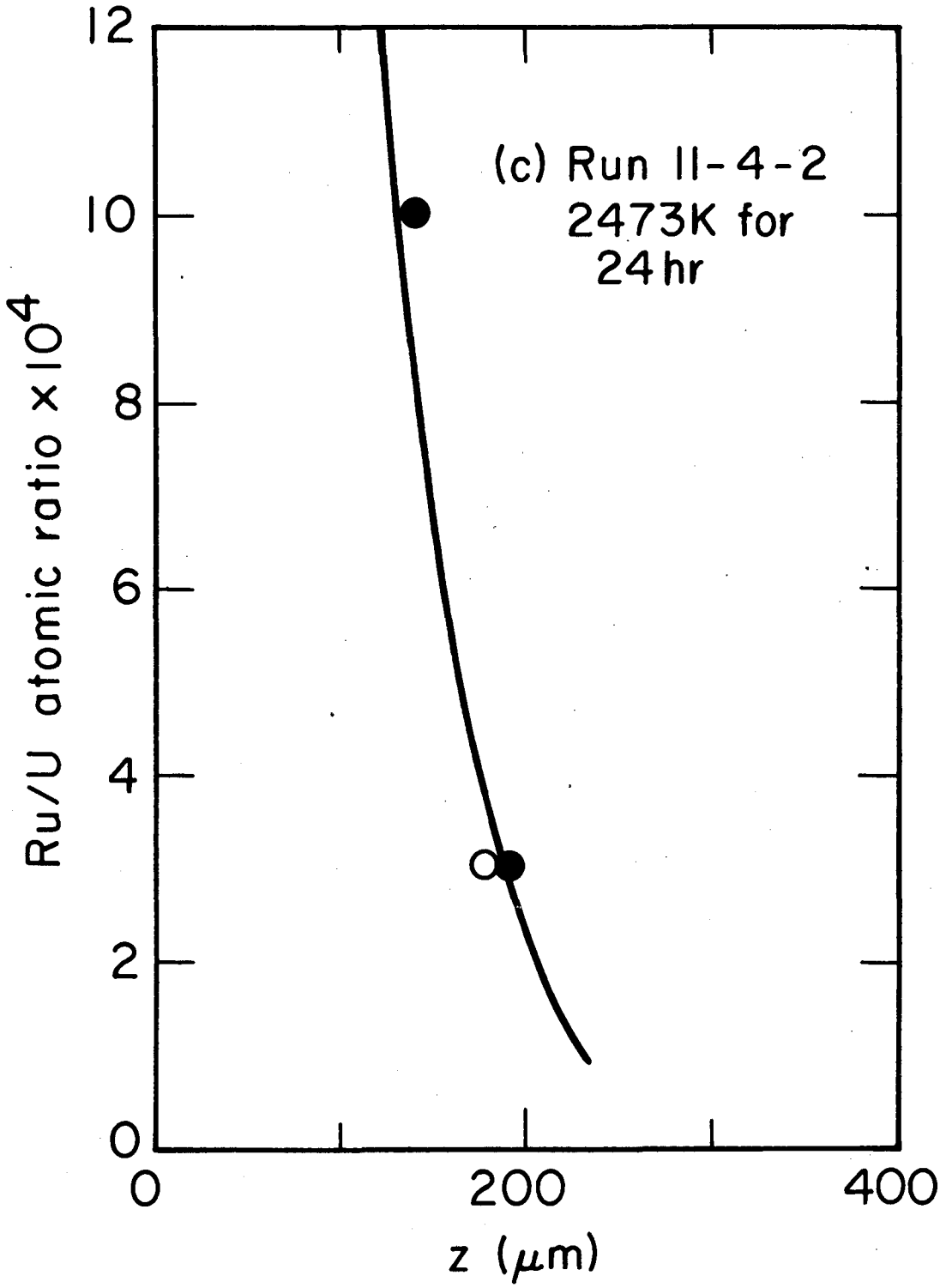

FIG 4c

XBL812-3652

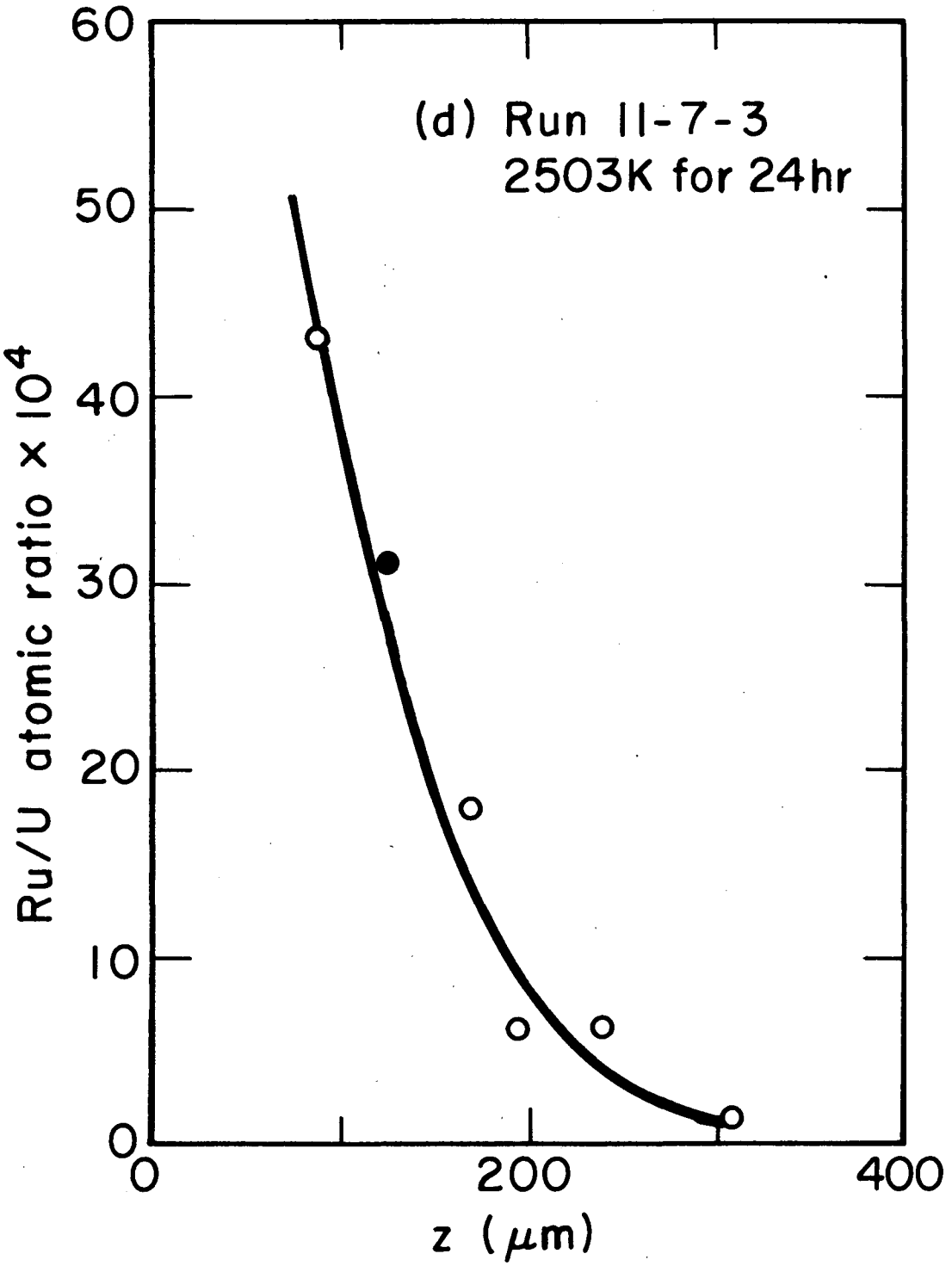

XBL812-3651

FIG 4d

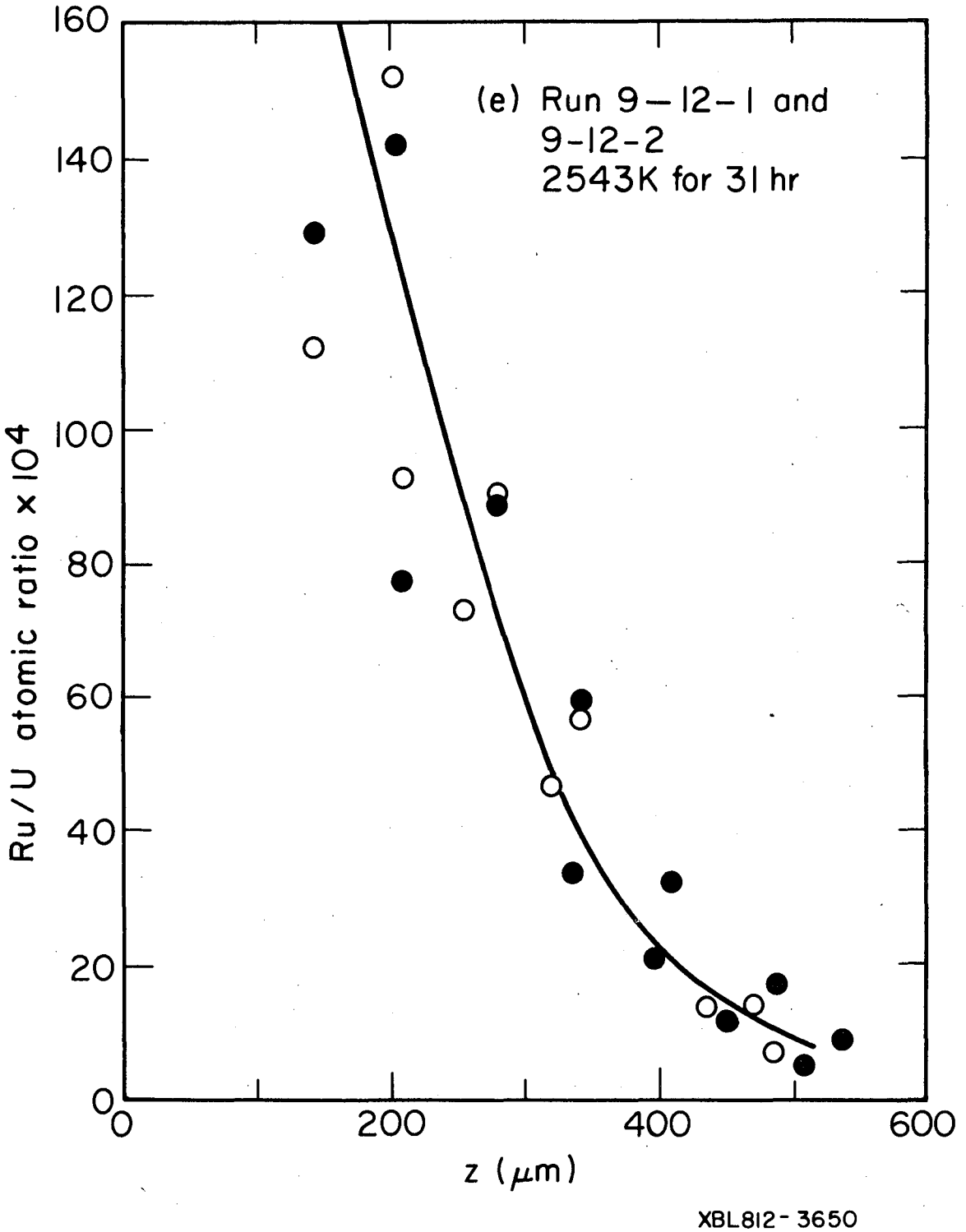
(e) Run 9—12—1 and
9-12-2
2543K for 31 hr
Ru/U atomic ratio x 10^4
z (μm)
0
20
40
60
80
100
120
140
160
200
400
600
XBL812-3650

FIG 4e

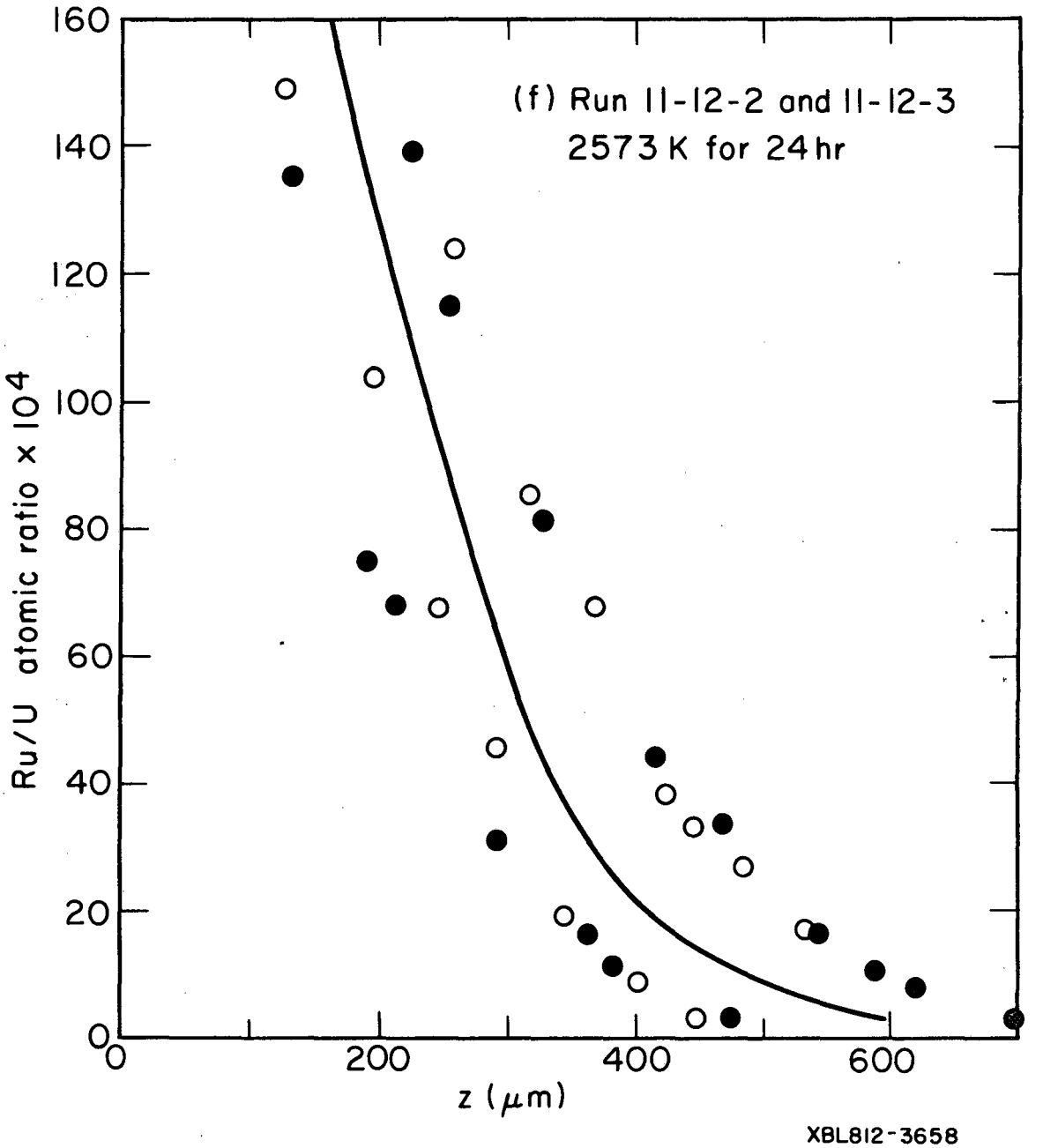
(f) Run 11-12-2 and 11-12-3
2573 K for 24 hr
Ru/U atomic ratio x 10^4
z (μm)
0
20
40
60
80
100
120
140
160
200
400
600
XBL812-3658

FIG 4f

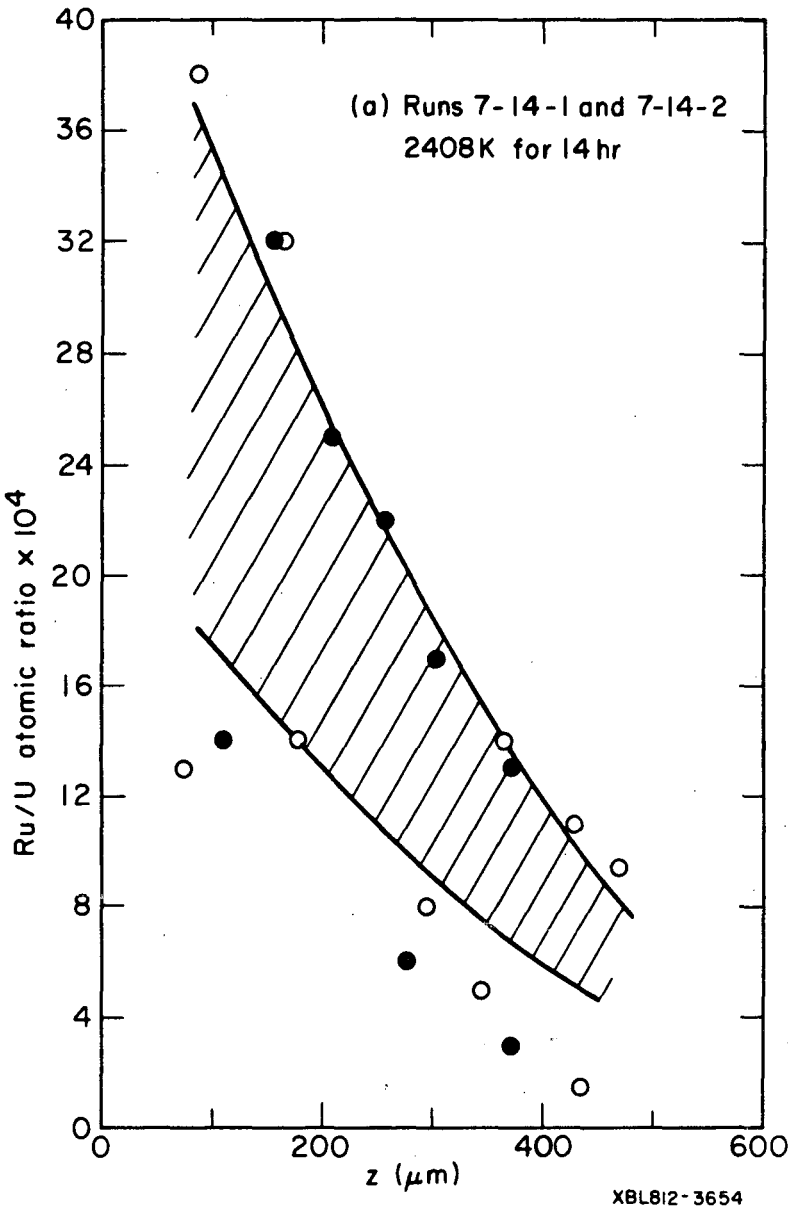

FIG 5 (a) - (c) Ruthenium distributions following isothermal anneals with molybdenum fittings; ○ pellet side of source plane; ● wafer side of source plane; ▨ model fit to data

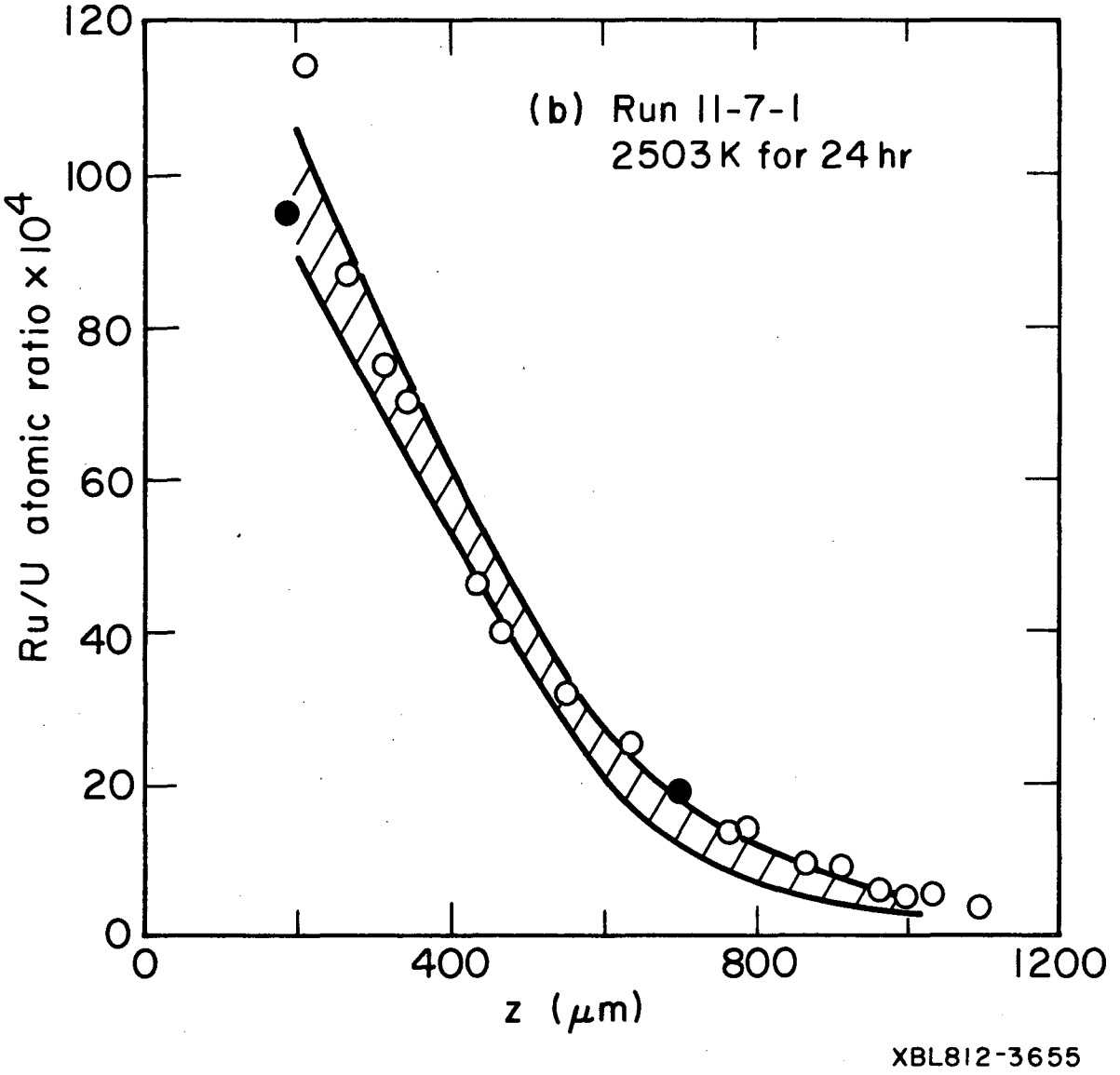
(b) Run 11-7-1
2503 K for 24 hr
Ru/U atomic ratio x 10^4
z (μm)
0
20
40
60
80
100
120
0
400
800
1200
XBL812-3655

FIG 5b

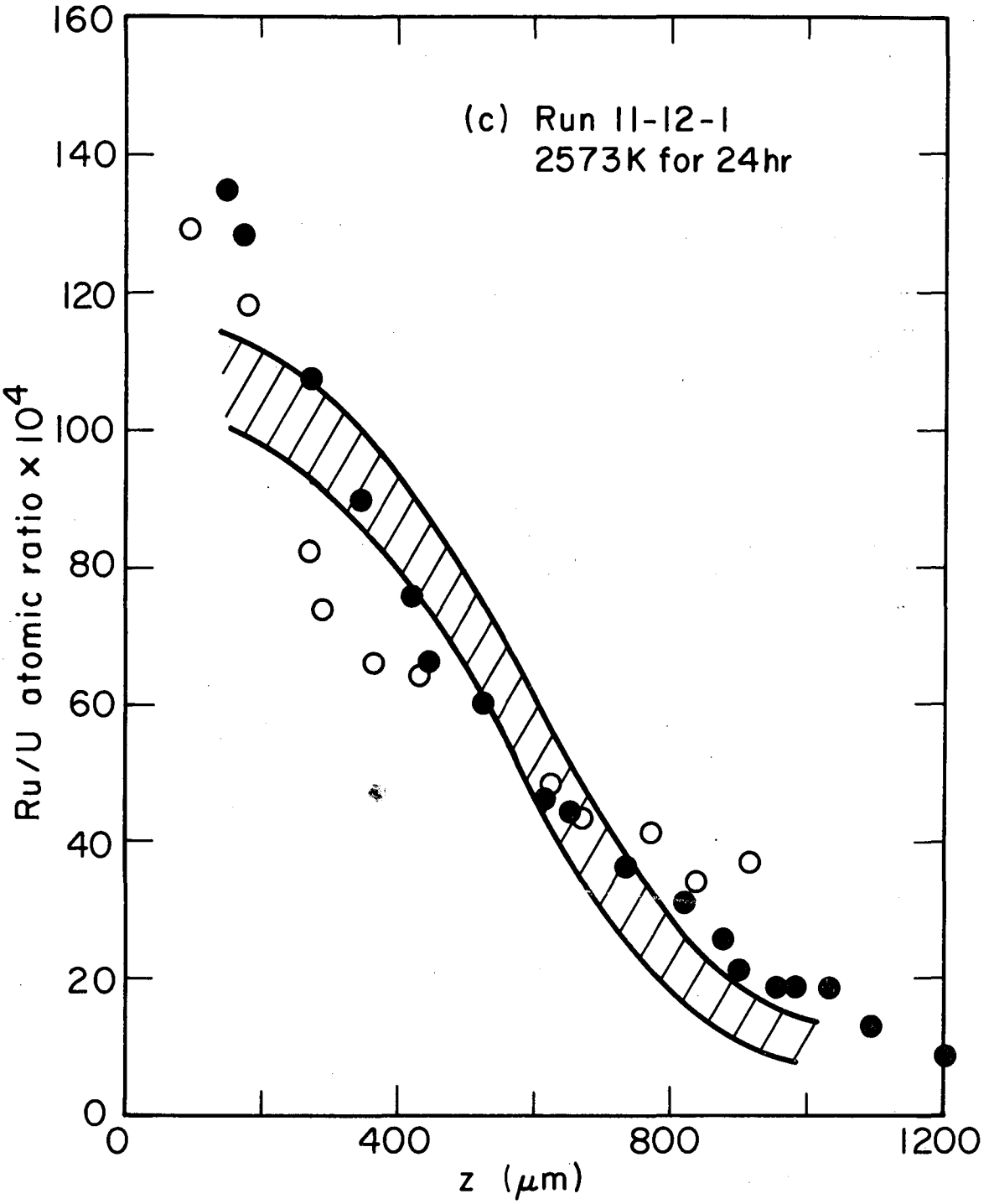

XBL 812-3657

FIG 5c

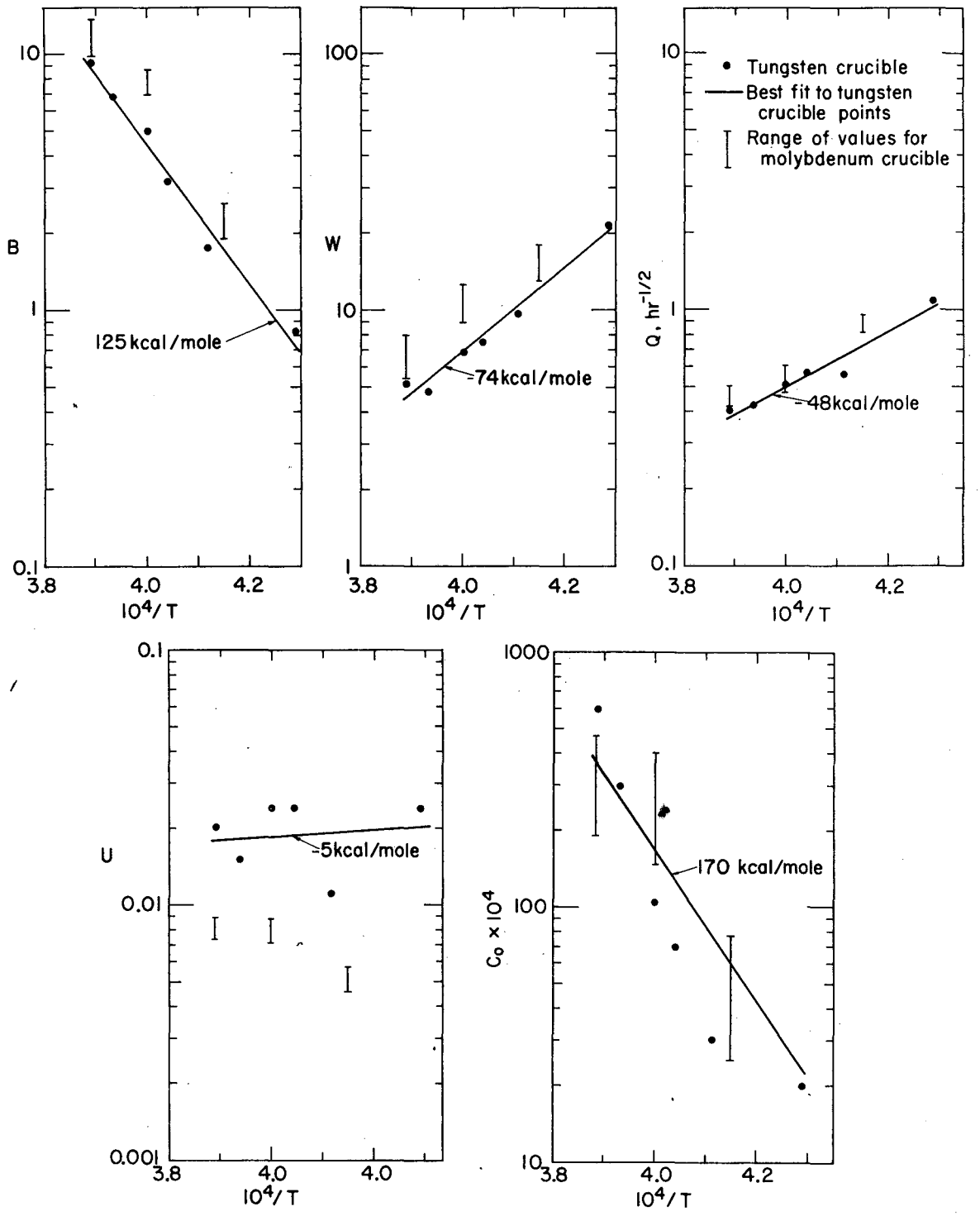

FIG 6 Model parameters obtained by fitting to isothermal ruthenium spreading data.

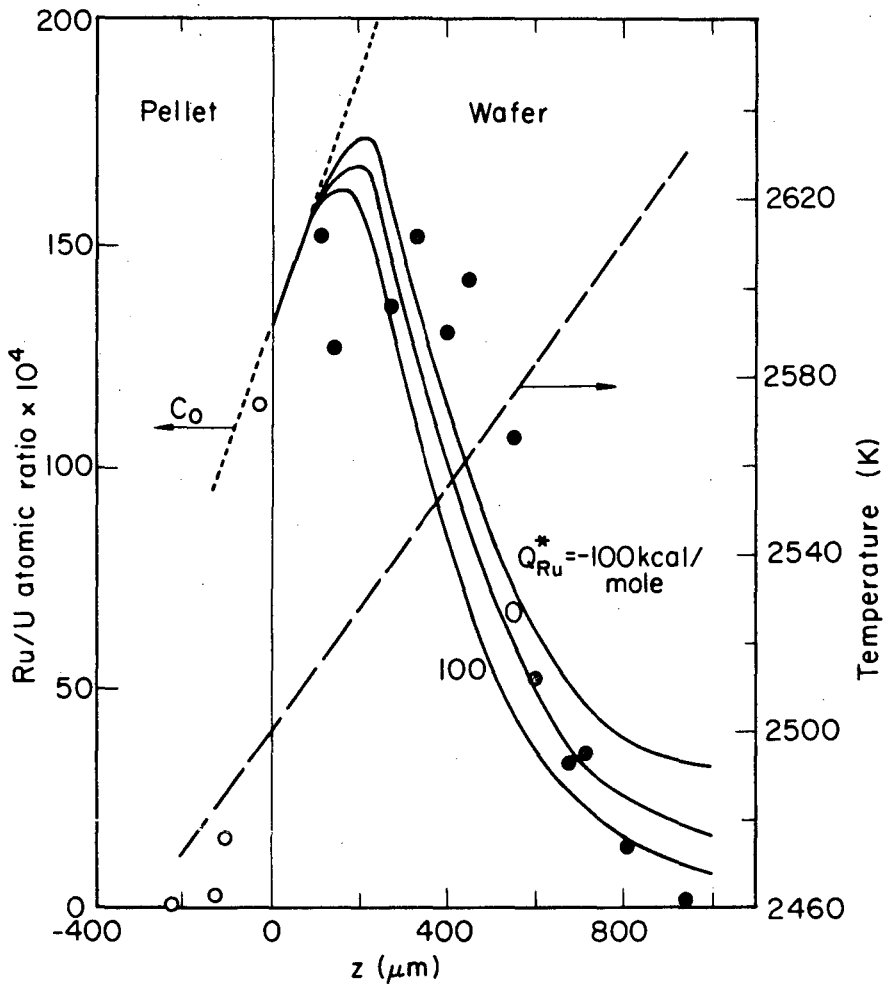

FIG 7 Application of the ruthenium interaction model to thermal gradient migration in UO_2. The solid lines are model fits for three values of the heat of transport. The long-dashed line is the calculated temperature profile and the short-dashed line is the saturation ruthenium concentration

This report was done with support from the Department of Energy. Any conclusions or opinions expressed in this report represent solely those of the author(s) and not necessarily those of The Regents of the University of California, the Lawrence Berkeley Laboratory or the Department of Energy.

Reference to a company or product name does not imply approval or recommendation of the product by the University of California or the U.S. Department of Energy to the exclusion of others that may be suitable.

TECHNICAL INFORMATION DEPARTMENT
LAWRENCE BERKELEY LABORATORY
UNIVERSITY OF CALIFORNIA
BERKELEY, CALIFORNIA 94720